https://doi.org/10.5194/egusphere-2026-3834
Preprint. Discussion started: 8 July 2026

Dynamical Mechanism behind the Southern Hemisphere Westerly Intensification during the Last Glacial Maximum: A Linkage between Sea-ice and Polar Front Jet

Hyeong-Gyu Kim[1], Joowan Kim[1,*], Sang-Yoon Jun[2], Seong-Joong Kim[2], Damwon So[1]

[1]Department of Atmospheric Science, Kongju National University, Gongju, 32588, South Korea
[2]Korea Polar Research Institute, Incheon, 21990, South Korea

Correspondence to: Joowan Kim (joowan.k@gmail.com)

Abstract. The Southern Hemisphere westerlies (SHW) play a pivotal role in modulating the global carbon cycle and climate feedback. However, their behavior during the Last Glacial Maximum (LGM) is debated owing to discrepancies between paleoclimate models and proxy records. While tropical upper-tropospheric cooling and Antarctic surface cooling exert opposing influences on the SHW, the detailed dynamical mechanisms through which Antarctic sea-ice expansion modulates large-scale atmospheric circulation are poorly understood. In this study, we investigated the dynamical mechanisms of austral winter SHW change under altered orbital and surface conditions with a series of climate model simulations. By conducting sensitivity experiments with varying Antarctic sea-ice concentrations, we isolated the thermodynamic effect of sea ice from the tropical cooling signal. Our results demonstrate that sea-ice-induced surface cooling drives the poleward intensification of the SHW through two distinct mechanisms. First, strong surface cooling steepens the meridional temperature gradient near the sea-ice edge, thereby directly maintaining the SHW intensity through thermal wind balance. Second, the enhanced baroclinicity amplifies eddy heat fluxes and storm track activity. The resulting increase in storm track activity drives a downward transfer of upper-tropospheric westerly momentum, reinforcing the surface westerlies. Through these mechanisms, the sea-ice-driven cooling outweighed the opposing equatorward influence of tropical cooling. This study provides a dynamical framework for understanding how sea-ice thermodynamic forcing drives large-scale circulation changes in the context of LGM climate conditions.

1 Introduction

Southern Hemisphere westerlies (SHW) are a fundamental component of the global climate system, mediating atmosphere-ocean interactions and driving the key physical processes in the Southern Ocean. They provide momentum for the Antarctic Circumpolar Current and drive the meridional overturning circulation by regulating the transport of water masses (Marshall and Speer, 2012; Rintoul, 2018; Toggweiler and Samuels, 1995). A poleward shift or intensification of the SHW enhances the wind-driven divergence of surface water, thereby increasing the rate of deep-water upwelling in the Southern Ocean (Hall and

https://doi.org/10.5194/egusphere-2026-3834
Preprint. Discussion started: 8 July 2026

Visbeck, 2002; Saunders et al., 2018; Toggweiler et al., 2006). This intensified upwelling exposes old, carbon-rich deep waters to the atmosphere and facilitates the ventilation of stored CO_2 (Anderson et al., 2009; Lauderdale et al., 2017; Lovenduski et al., 2007; Menviel and Spence, 2024; Toggweiler and Russell, 2008). Furthermore, the SHW is closely linked to the large-scale hydrological cycle, modulating precipitation patterns across the Southern Hemisphere (Fogt and Marshall, 2020; Hodgson and Sime, 2010; Lamy et al., 2010; Saunders et al., 2012; Yin, 2005). Thus, understanding the variability of the SHW is essential for investigating past climate transitions and future climate change.

In recent decades, observational records have indicated that the SHW has shifted poleward and intensified significantly. This trend is robust across multiple data sources, including satellite measurements (Fu et al., 2006; Young and Ribal, 2019), surface observations, proxy records (Abram et al., 2014; Dixon et al., 2011; Marshall, 2003; O'Connor et al., 2021; Tetzner et al., 2025; Thompson and Solomon, 2002; Visbeck, 2009), and reanalysis datasets (Fogt and Marshall, 2020; Goyal et al., 2021; Hogg et al., 2015; Perren et al., 2025; Swart and Fyfe, 2012). Most notably, a recent 140-year reconstruction based on an ice core revealed that the current strengthening of the Pacific SHW is unprecedented in the instrumental record (Tetzner et al., 2025). These changes are primarily attributable to the combined effects of increased greenhouse gas concentrations (Barnes and Polvani, 2013; Zheng et al., 2013) and stratospheric ozone depletion (Son et al., 2010; Thompson and Solomon, 2002). In 21st-century projections, ozone recovery causes an equatorward shift in the SHW and partially offsets the poleward forcing from global warming (Son et al., 2008). However, climate models project that rising greenhouse gases will override the equatorward influence of ozone recovery, driving continued poleward intensification (Chavaillaz et al., 2013; Deng et al., 2022; Goyal et al., 2021; Ivanciu et al., 2022; Swart and Fyfe, 2012; Thompson et al., 2011; Yin, 2005). Given the importance of these shifts, a comprehensive understanding of SHW behavior is required beyond the conventional observational era (Abram et al., 2014; Fogt and Marshall, 2020).

In this regard, paleoclimate archives provide invaluable insight into global climate variability and its underlying mechanisms (Harrison et al., 2015; Kageyama et al., 2024; Tierney et al., 2020b). Extensive analyses of paleoclimate proxy data indicate that the SHW underwent significant modifications during glacial periods, generally intensifying or shifting equatorward compared to interglacials (Chen et al., 2024; Kohfeld et al., 2013; Lamy et al., 2014; Quade and Kaplan, 2017; Spoth et al., 2023). Synthesis studies of the proxy data suggest that the SHW shifted equatorward by 3°–5° during the Last Glacial Maximum (Gottschalk et al., 2019; Kohfeld et al., 2013). However, directly inferring SHW changes from these paleoclimate records remains challenging. For example, Kohfeld et al. (2013) noted that alternative scenarios such as a weakening or poleward shift of the SHW could not be excluded because the same proxy signatures can emerge from multiple atmospheric circulation patterns. Recent proxy-based reconstructions support the weakening and equatorward displacement of the SHW during glacial conditions (Gray et al., 2023; Perren et al., 2020). In contrast, reproducing this reconstructed equatorward shift remains a persistent challenge in paleoclimate modeling as described below.

https://doi.org/10.5194/egusphere-2026-3834
Preprint. Discussion started: 8 July 2026

The SHW response exhibits a large inter-modal spread across various paleoclimate simulations of the LGM (Chavaillaz et al., 2013; Kim et al., 2002, 2017; Kim and Lee, 2009; Menviel et al., 2008; Otto-Bliesner et al., 2006; Rojas et al., 2009; Sime et al., 2013, 2016; Toggweiler et al., 2006; Wyrwoll et al., 2000). Discrepancies in the magnitude and direction of SHW changes remain unresolved even in recent studies (Du et al., 2024; Gottschalk et al., 2019; Gray et al., 2023; Kim and Son, 2020). However, closer inspection reveals that these inconsistencies are not arbitrary, but dynamically linked to the surface boundary conditions. Generally, the Paleoclimate Modeling Intercomparison Project (PMIP) models for the LGM show an equatorward weakening of the SHW driven by upper-tropospheric tropical cooling, which contracts the tropical circulation (Rojas, 2013). In contrast, some models simulate poleward intensification accompanied by near-surface Antarctic cooling that is strongly coupled to sea-ice expansion (Chavaillaz et al., 2013; Rojas, 2013; Rojas et al., 2009). Sime et al. (2016) demonstrated that models with an accurate representation of the pre-industrial sea-ice edge exhibited a distinct poleward shift of the SHW in response to LGM sea-ice expansion. This finding implies that when coupling is robust in the model, the expanded sea ice drives a poleward displacement of the jet, opposing the equatorward thermal forcing associated with tropical cooling in glacial climates (Chase et al., 2025).

While these thermal arguments identify competing drivers in the models, a detailed explanation of the dynamical processes is needed, particularly regarding the eddy-mean flow interactions that govern the latitudinal position and intensity of the SHW. Recently, an idealized model study by Kim and Son (2023) hinted at the role of the tropospheric eddy flux in modulating the SHW under prescribed thermal forcings. Building upon this insight, this study aims to elucidate the dynamical mechanisms of the poleward intensification of the SHW during the LGM. To achieve this, we simulated the SHW under the influence of two competing thermal forcings, near-surface Antarctic cooling and upper-tropospheric tropical cooling, using climate model experiments. Subsequently, a diagnostic framework based on the momentum budget analysis was employed to investigate how these two thermal forcings influence atmospheric circulation through the eddy-mean flow interaction and ultimately determine the latitudinal position and intensity of the SHW. Finally, the specific impact of the Antarctic sea ice boundary condition was isolated to quantify the sensitivity of the SHW to this surface forcing.

The remainder of this paper is organized as follows: Section 2 describes the experimental design and model configuration. Section 3 presents the simulation results and a detailed dynamical analysis. Section 4 summarizes the main findings and conclusions. Finally, Section 5 discusses the broader implications of our findings, including a critical assessment of the potential uncertainties and limitations inherent in the model framework.

https://doi.org/10.5194/egusphere-2026-3834
Preprint. Discussion started: 8 July 2026

2 Experimental design

2.1 Model descriptions

All numerical simulations were performed using the Community Earth System Model version 1.2 (CESM1.2; Hurrell et al., 2013). This fully coupled global climate model integrates atmospheric, oceanic, sea-ice, and land surface components through the CPL7 coupler. The atmospheric component was the Community Atmosphere Model version 5 (CAM5; Neale et al., 2012) with CAM4 physics (Neale et al., 2010), which employed a finite-volume (FV) dynamical core. The model was configured with a horizontal resolution of approximately 1.9° × 2.5° (latitude × longitude) and 26 hybrid sigma-pressure vertical levels extending from the surface to approximately 2 hPa. The ocean and sea-ice components operated on a nominal 1° horizontal grid with the displaced grid pole positioned over Greenland (gx1v6). The ocean component was the Parallel Ocean Program version 2 (POP2; Smith et al., 2010) with 60 vertical levels, and the sea-ice component was the Community Ice Code version 4 (CICE4; Hunke and Lipscomb, 2010), which includes elastic-viscous-plastic dynamics and thermodynamic parameterization schemes. The land surface was simulated using the Community Land Model version 4 (CLM4; Oleson et al., 2010; Lawrence et al., 2011).

Two fully coupled equilibrium simulations were performed to establish the baseline climate states: pre-industrial (PI) and LGM control simulations. The PI simulation followed the CMIP5 experimental design for pre-industrial control (Taylor et al., 2012), representing pre-industrial climate conditions circa 1850. Atmospheric trace gas concentrations were fixed at CO_2 = 284.7 ppm, CH_4 = 791.6 ppb, and N_2O = 275.7 ppb, with aerosols and ozone prescribed using standard 1850 climatology. This configuration served as the baseline representing the quasi-equilibrium climate state prior to substantial anthropogenic emissions.

The LGM simulation followed the PMIP3 protocol (Braconnot et al., 2012), with the boundary conditions set for 21,000 years before the present (21 ka). Atmospheric trace gases were reduced to LGM levels: CO_2 to 185 ppm (Monnin et al., 2001), CH_4 to 350 ppb (Dällenbach et al., 2000), and N_2O to 200 ppb (Flückiger et al., 1999), resulting in reduced net radiative forcing. The ice sheet topography was initialized based on the PMIP3 blended reconstruction (Abe-Ouchi et al., 2015), providing the high surface albedo essential for reproducing the global cooling characteristic of the glacial maximum. The orbital parameters were set to 21 ka (Berger, 1978).

Both simulations were integrated for over 250 years. The first 200 years were discarded as a spin-up period to ensure that the model reached equilibrium, and the last 50 years were used for the analysis. The analysis primarily focused on the austral winter (June–August; JJA), as the interaction between large-scale atmospheric circulation and sea ice is known to be most robust during the cold season (Ayres et al., 2022; Kidston et al., 2011; Simpkins et al., 2012). Consistent with this seasonal dependency, Kim and Son (2020) demonstrated a distinct seasonal contrast in jet shift response between summer and winter,

https://doi.org/10.5194/egusphere-2026-3834
Preprint. Discussion started: 8 July 2026

suggesting that near-surface Antarctic cooling drives the inter-model differences. Furthermore, given the critical role of sea ice in modulating the Antarctic cooling and the overall SHW response (Kim et al., 2017; Sime et al., 2016), sensitivity experiments were conducted to isolate the specific impact of sea-ice forcing.

2.2 Sea ice sensitivity experiments

To isolate the dynamical impact of Antarctic sea-ice expansion on the SHW while excluding complex ocean-atmosphere feedbacks, a suite of atmosphere-only sensitivity experiments was performed using the standalone atmospheric component. In these experiments (hereafter ICEα), the prescribed sea-ice concentration (SIC) was constructed by superimposing the linearly scaled Antarctic sea-ice anomalies (derived from the LGM minus PI sea-ice concentration difference) onto the pre-industrial climatology. The prescribed SIC for each experiment was calculated as follows:

$$SIC_{ICE} = min(SIC_{PI} + \alpha(SIC_{LGM} - SIC_{PI}), 1) \quad (1),$$

where SIC_{PI} denotes the Hadley-based PI climatology (Rayner et al., 2003) and SIC_{LGM} represents the PMIP3 protocol-based LGM boundary conditions (Abe-Ouchi et al., 2015). The weighting factor α modulates the magnitude of the sea-ice expansion, set to 0.5, 0.75, 1.0, and 1.25 (corresponding to 50%–125% of the full LGM sea-ice anomaly).

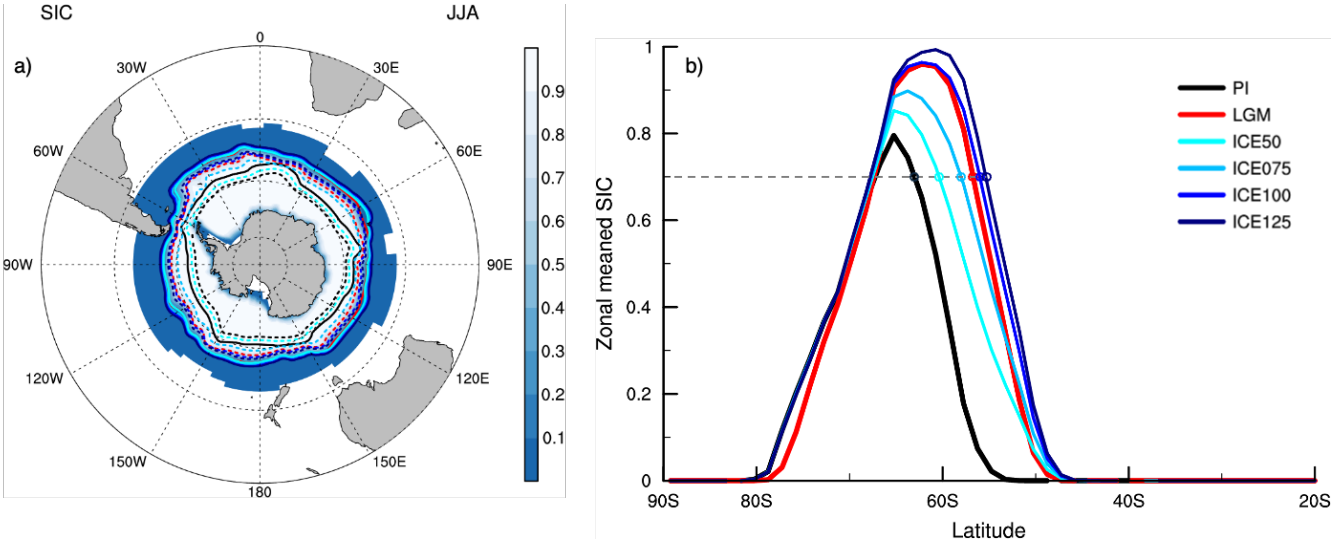

Figure 1: (a) Austral winter (JJA) sea-ice concentration (SIC) in the Southern Hemisphere. Shading represents the spatial distribution of SIC for the LGM experiment. Solid and dashed contours denote the sea-ice boundaries where the SIC is 0.15 and 0.7, respectively, for each experiment (line colors correspond to the legend in b). (b) Zonal-mean SIC profiles for each simulation. The horizontal gray dashed line marks the 0.7 threshold, and the open circles indicate the corresponding latitude for each experiment, which serves as a reference metric in subsequent analyses (Fig. 10).

https://doi.org/10.5194/egusphere-2026-3834
Preprint. Discussion started: 8 July 2026

Figure 1 illustrates the austral winter sea-ice boundaries for control and sensitivity experiments. This boundary condition enables us to assess the SHW response to the Antarctic sea-ice coverage. To focus exclusively on this sea-ice effect, the sea surface temperature (SST) was taken from the PI experiment. Each sensitivity experiment was conducted over 50 years. Unlike fully coupled runs, these atmosphere-only simulations lack the slow thermal inertia of a dynamic ocean, allowing the model to reach equilibrium almost immediately. Given the rapid adjustment of atmospheric circulation to surface boundary forcing, the entire 50-year period was utilized for analysis to ensure robust climatological statistics. All the experimental configurations are summarized in Table 1.

Table 1. Summary of the experimental design

Experiment	Type	SST/SIC reference	Feature / Purpose
PI	Coupled	Prognostic (Internally simulated)	Pre-industrial baseline simulation
LGM	Coupled	Prognostic (Under PMIP3 protocols)	Last Glacial Maximum baseline simulation
ICE50	Atmosphere-only	prescribed PI + 50% of Δ SIC	Sensitivity run applying 0.5 × (LGM-PI) SIC difference
ICE75	Atmosphere-only	prescribed PI + 75% of Δ SIC	Sensitivity run applying 0.75 × (LGM-PI) SIC difference
ICE100	Atmosphere-only	prescribed PI + 100% of Δ SIC	Sensitivity run applying 1.0 × (LGM-PI) SIC difference
ICE125	Atmosphere-only	prescribed PI + 125% of Δ SIC	Sensitivity run applying 1.25 × (LGM-PI) SIC difference

* Note: Δ SIC represents the difference of sea ice concentration between PMIP3 protocol-based LGM boundary conditions and Hadley-based PI.

2.3 Diagnostic framework

To elucidate the physical mechanisms driving the atmospheric circulation response, changes in atmospheric baroclinicity were analyzed with a focus on eddy-mean flow processes. Atmospheric baroclinicity was quantified using the maximum Eady growth rate (Lindzen and Farrell, 1980). This metric represents the maximum theoretical growth rate of baroclinic eddies and is defined as:

https://doi.org/10.5194/egusphere-2026-3834
Preprint. Discussion started: 8 July 2026

$$EGR = 0.31 \frac{|f|}{N}\left|\frac{dU}{dz}\right| \quad (2),$$

where f is the Coriolis parameter, N is the Brunt-Väisälä frequency representing static stability, and dU/dz denotes the vertical shear of the zonal wind. Given that the vertical wind shear is governed by the thermal-wind relationship, EGR serves as a measure of the lower-tropospheric baroclinicity, reflecting the strength of the meridional temperature gradient.

To identify the location, intensity, and thermal effects of storm tracks, the synoptic-scale transient eddy activity was characterized. The instantaneous 6-hourly meridional velocity and temperature fields were filtered using a 2–7-day band-pass Lanczos filter to isolate high-frequency fluctuations associated with synoptic weather systems. Following Chang et al. (2002), storm track activity was defined as the variance of the band-pass-filtered meridional wind at 300 hPa. Low-level baroclinicity was assessed using the meridional eddy heat flux at 850 hPa.

To diagnose the dynamical role of transient eddies in driving zonal-mean flow changes, the Eliassen-Palm (EP) flux formalism was employed. This diagnostic framework provides a vector representation of the effective wave activity flux and its interaction with the mean flow (Andrews et al., 1987; Holton, 2004). According to the transformed Eulerian mean (TEM) zonal momentum equation in spherical log-pressure coordinates, the divergence of these eddy fluxes acts as a force on zonal wind:

$$\bar{u}_t + \bar{v}^*\left[(a\cos\phi)^{-1}(\bar{u}\cos\phi)_\phi - f\right] + \bar{w}^*\bar{u}_z - \bar{X} = (\rho_0\, a\cos\phi)^{-1}\nabla\cdot F \quad (3)$$

where $\bar{v}^*$ and $\bar{w}^*$ denote the meridional and vertical components of the residual mean circulation, respectively; X represents the unresolved mechanical friction; and F is the EP flux. All other notations follow the formalism detailed in Andrews et al. (1987). The meridional and vertical components of the EP flux vector, $F = (0, F_\phi, F_z)$, are defined as:

$$F_\phi \equiv \rho_0\, a\cos\phi\,(\bar{u}_z\overline{v'\theta'}/\bar{\theta}_z - \overline{v'u'}) \quad (4)$$

$$F_z \equiv \rho_0\, a\cos\phi\left\{\left[f - (a\cos\phi)^{-1}(\bar{u}\cos\phi)_\phi\right]\overline{v'\theta'}/\bar{\theta}_z - \overline{w'u'}\right\} \quad (5)$$

Crucially, the eddy flux terms (e.g., $\overline{v'u'}$ and $\overline{v'\theta'}$) were computed using 6-hourly instantaneous output to explicitly resolve transient disturbances. For visual clarity across the upper atmospheric levels, the EP flux vectors were scaled by $e^{z/H}$ in the

https://doi.org/10.5194/egusphere-2026-3834
Preprint. Discussion started: 8 July 2026

upper atmosphere (Jucker, 2021). We focused on the divergence of the EP flux to identify how sea-ice-induced wave activity forcing drives changes in the position and intensity of the SHW.

3 Dynamical responses of the Southern Hemisphere westerlies

3.1 Thermal wind response of the tropospheric jets

During the austral winter, both the LGM and PI simulations successfully capture the characteristic structures of the Southern Hemisphere tropospheric circulation, featuring a deep westerly wind belt centered between 50°S and 60°S and a distinct upper-tropospheric subtropical jet near 30°S (Figs. 2a and 2b). The latitudinal positions of both jet systems coincide with the regions of strong meridional temperature gradients. Because our primary interest lies in the mid-to-high latitude circulation driven by transient eddies, which exhibits a deep structure extending to the surface, the term "SHW" hereafter refers specifically to this eddy-driven polar front jet.

The transition to LGM boundary conditions induced substantial changes in the thermal structure of the Southern Hemisphere, characterized by two major cooling regions: the tropical upper troposphere and the Antarctic lower troposphere (Fig. 2c). The tropical upper-tropospheric cooling represents a thermodynamic response to radiative forcing, as the temperature profile follows the moist adiabat—a reversal of the upper-tropospheric warming amplification projected under modern climate change (Santer et al., 1996, 2005). The LGM cooling pattern is consistent with robust clumped-isotope palaeothermometry constraints (Banerjee et al., 2022). This upper-level cooling reduced the meridional temperature gradient, leading to a distinct weakening of the subtropical jet (Fig. 2d). In contrast, intense Antarctic surface cooling arose from LGM boundary conditions, particularly the expanded sea-ice cover and altered ice-sheet topography (Chavaillaz et al., 2013). Consistent with proxy-assimilated reconstructions (Tierney et al., 2020a), this severe cooling is most pronounced along the sea-ice margins. Consequently, it significantly steepens the high-latitude meridional temperature gradient (Fig. 2c; Wyrwoll et al., 2000), driving a poleward displacement of the SHW. The resulting zonal wind anomaly exhibited a distinct dipole pattern, intensifying along the poleward flank of the jet (Fig. 2d).

https://doi.org/10.5194/egusphere-2026-3834
Preprint. Discussion started: 8 July 2026

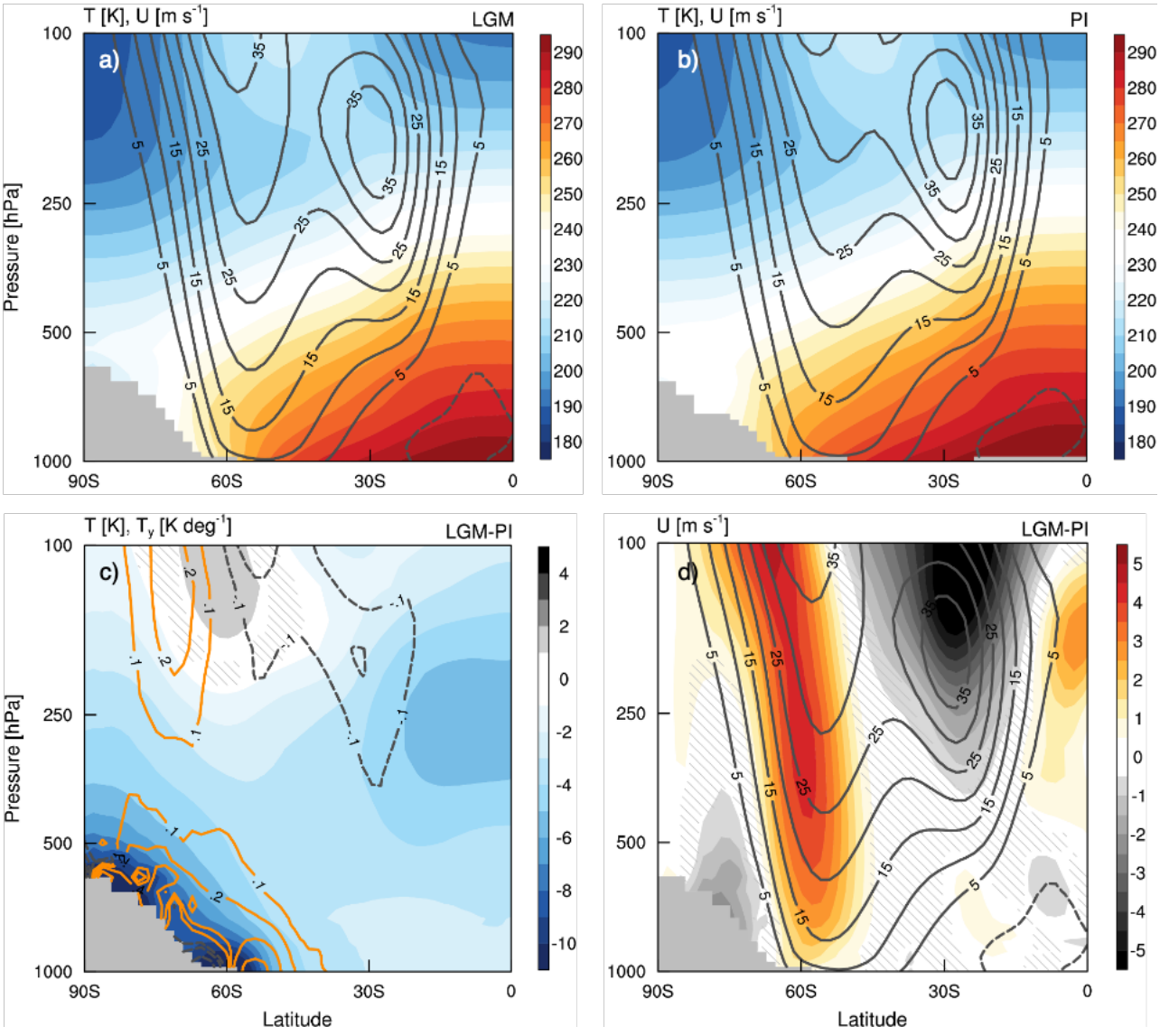

Figure 2: Zonal-mean atmospheric structures during austral winter (JJA). Vertical cross-sections of temperature (K; shading) and zonal wind (m s^{-1}; contours) for (a) LGM and (b) PI. (c) Differences (LGM minus PI) in temperature (K; shading) and in the meridional temperature gradient (K deg^{-1}; contours). Contour intervals for the gradient difference are set at ±0.1, ±0.2, ±0.4, and ±0.8 K deg^{-1}. (d) Differences in zonal wind (m s^{-1}; shading) overlaid with LGM climatological zonal wind (m s^{-1}; contours). Solid (dashed) contours denote positive (negative) values. Hatching indicates regions where the shaded differences are not statistically significant at the 99% confidence level, based on a Student's *t*-test. Gray areas represent topography.

During austral winter, the mid-tropospheric SHW formed a largely continuous circumpolar band centered near ~55°S, aligning closely with regions of maximum meridional thickness gradient in both simulations (Figs. 3a and 3b). Under LGM conditions, intense Antarctic surface cooling contracted the lower-tropospheric layer. Because this cooling was disproportionately stronger than in the mid-latitudes, it sharply steepened the high-latitude meridional gradient thickness along the expanded sea-ice

https://doi.org/10.5194/egusphere-2026-3834
Preprint. Discussion started: 8 July 2026

margin. Consistent with thermal wind balance, this differential cooling directly drove a distinct poleward intensification of the westerlies over the Southern Ocean (Fig. 3c).

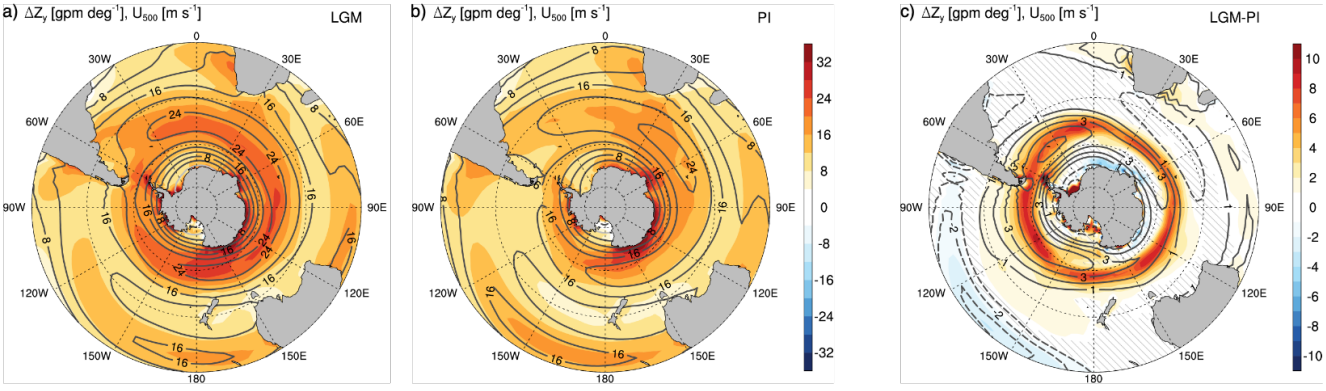

Figure 3: Lower-tropospheric baroclinicity and 500 hPa zonal wind during austral winter (JJA). The meridional gradient of geopotential thickness (ΔZ_y) between 500 and 1000 hPa (gpm deg^{-1}; shading) and the zonal wind at 500 hPa (m s^{-1}; contours) for (a) LGM, (b) PI, and (c) the difference (LGM minus PI). In panel (c), solid (dashed) contours indicate positive (negative) zonal wind differences, with contour levels at ±1, ±2, ±3, ±4, and ±5 m s^{-1}. Hatching indicates regions where the shaded differences are not statistically significant at the 99% confidence level, based on a Student's *t*-test.

This poleward intensification extended to the near-surface circulation. In accordance with geostrophic balance, the 1000 hPa zonal wind aligned with the meridional sea-level pressure (SLP) gradient (Fig. 4). While the vertical coherence between the surface and mid-troposphere jet responses highlights the deep equivalent barotropic structure of the SHW, the maintenance of this near-surface shift involves dynamical processes beyond a direct thermal wind response. This necessitates an examination of eddy-mean flow interactions, which are detailed in Section 3.2 to further elucidate the coupling between thermal forcing and surface wind changes.

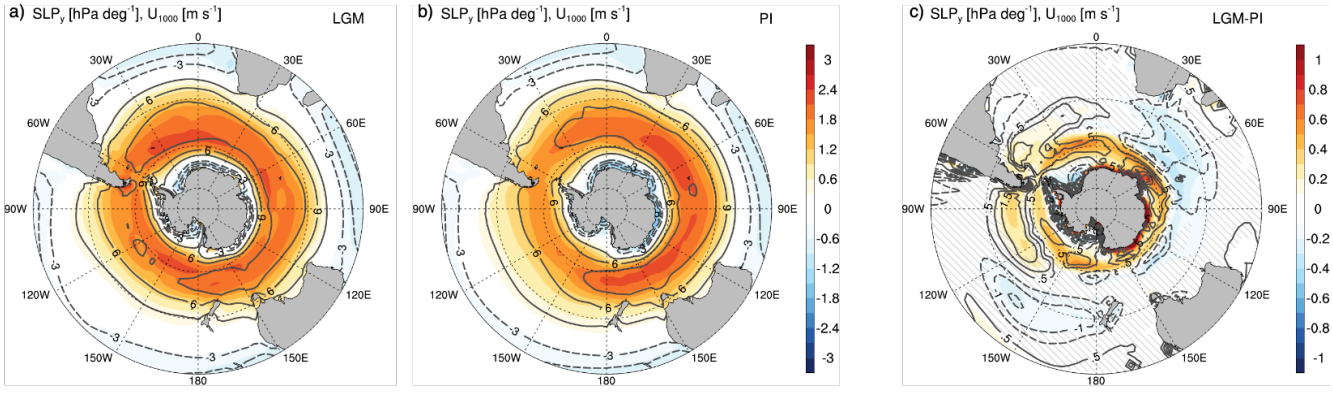

Figure 4: Meridional gradient of sea level pressure (SLP_y) and 1000 hPa zonal wind during austral winter (JJA). SLP_y (hPa deg^{-1}; shading) overlaid with the zonal wind at 1000 hPa (m s^{-1}; contours) for (a) LGM, (b) PI, and (c) the difference (LGM minus PI). In

https://doi.org/10.5194/egusphere-2026-3834
Preprint. Discussion started: 8 July 2026

panel (c), solid (dashed) contours indicate positive (negative) zonal wind differences, with contour levels at ±0.5, ±1, ±1.5, ±2, and ±2.5 m s^{-1}. Hatching indicates regions where the shaded differences are not statistically significant at the 99% confidence level, based on a Student's *t*-test.

In the LGM simulation, the substantial Antarctic cooling was governed by elevated continental ice sheets and expanded sea-ice (Chavaillaz et al., 2013; Kim et al., 2017). While thicker ice sheets predominantly cool the Antarctic interior (Buizert et al., 2021), widespread cooling over the Southern Ocean stems directly from the extensive sea-ice coverage (Rojas et al., 2009). Consequently, sea ice acted as the primary driver of the lower-tropospheric thermal forcing that modulates the SHW response (Fig. 5a), as its expanded margin directly reached the core latitudes of the westerlies. This intense subpolar cooling was driven by the insulating effect of the ice cover, which drastically suppressed the upward surface heat flux, comprising both sensible and latent heat fluxes (Fig. 5b). By effectively suppressing the oceanic heat supply to the atmosphere (Landrum and Holland, 2022; Maykut, 1986), the sea ice induced the severe atmospheric cooling over the Southern Ocean (Mitchell and Senior, 1989), thereby steepening the meridional temperature gradient and dynamically sustaining the poleward intensification of the SHW.

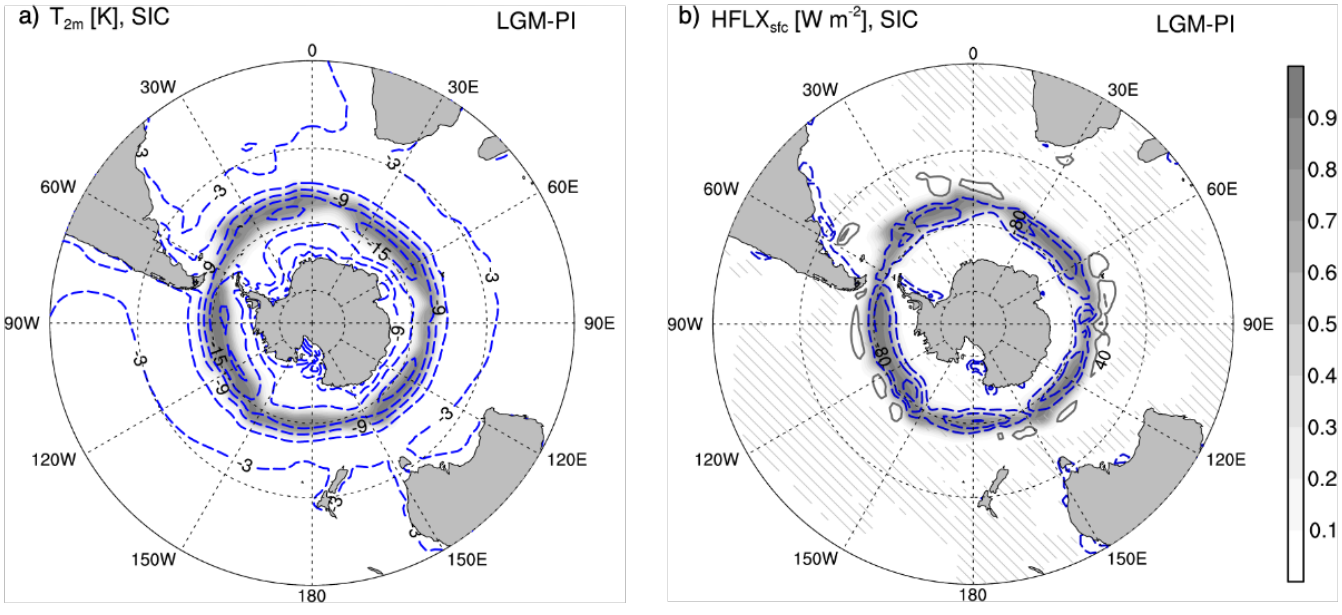

Figure 5: Differences in sea-ice concentration (SIC; shading) between the LGM and PI simulations (LGM minus PI) during austral winter (JJA), overlaid with differences in (a) 2-meter temperature (K; contours), and (b) surface heat flux (W m^{-2}; contours). The surface heat flux represents the sum of sensible and latent heat fluxes. Solid (dashed) contours indicate positive (negative) values, with contour levels set at ±3, ±6, ±9, ±12, and ±15 K for panel (a) and ±40, ±80, and ±120 W m^{-2} for panel (b). Hatching indicates regions where the contoured differences are not statistically significant at the 99% confidence level, based on a Student's *t*-test.

https://doi.org/10.5194/egusphere-2026-3834
Preprint. Discussion started: 8 July 2026

3.2 Mechanism of near-surface westerly change

The latitude at which the meridional temperature gradient maximizes is crucial for modulating the SHW and its associated baroclinic zone (Sime et al., 2016). Idealized studies have shown that an enhanced thermal contrast emerging poleward of the westerlies exerts a substantial influence on baroclinic wave development and displaces the jet (Brayshaw et al., 2008; Chen et al., 2010). In the present simulations, the extensive surface cooling induced by the Antarctic sea-ice expansion markedly steepened the lower-tropospheric temperature gradients at high latitudes. This sharpened thermal contrast created a highly baroclinic environment, thereby demanding greater transient eddy heat transport to restore thermal balance (Bader et al., 2013; Menéndez et al., 1999).

Driven by this steepened temperature gradient, vertical wind shear strengthened significantly over the Southern Ocean. This intensification was intrinsically coupled with widespread baroclinic instability, as evidenced by the enhanced Eady growth rate concentrated on the poleward flank of the SHW (Fig. 6a; Eq. 2). As elucidated by Kidston et al. (2011), the enhanced Eady growth rate on the jet's poleward flank drives the poleward shift of the SHW by amplifying the transient eddy generation. Reflecting this process, the associated lower-troposphere eddy heat flux in our simulation intensified at higher latitudes (Fig. 6b), consistent with the Antarctic cooling experiments by Kim and Son (2023). This enhanced eddy heat flux partially offset the steepened meridional temperature gradient and drives upward propagation of wave activity (Eq. 4). Consequently, this destabilized baroclinic environment supported the growth of intensified baroclinic waves. These waves propagated upward and were steered eastward by the background westerly flow, establishing an intensified upper-level storm track poleward of its PI position (Fig. 6c).

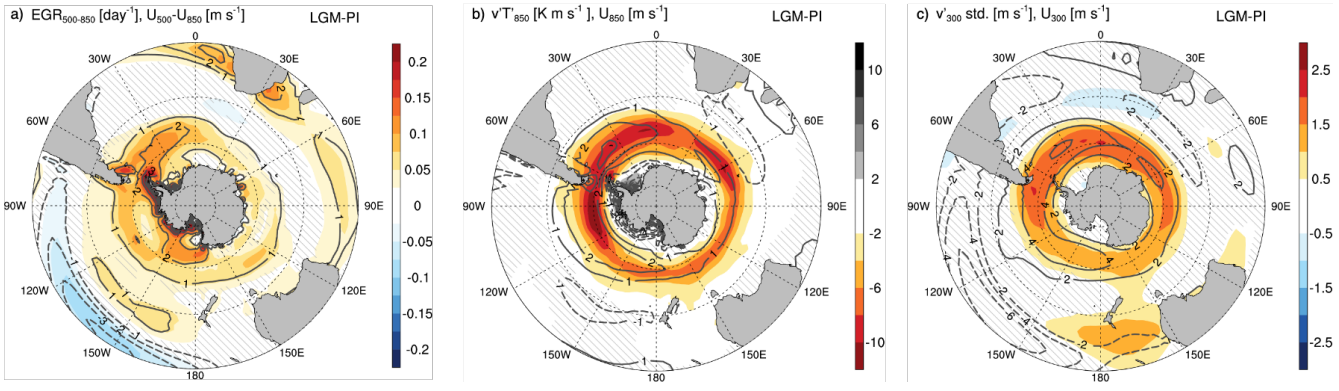

Figure 6: Response of baroclinicity and storm tracks to the LGM boundary conditions (LGM minus PI) during austral winter (JJA). Shown are the differences in (a) lower-tropospheric Eady growth rate (shading; day^{-1}) and vertical wind shear (contours; m s^{-1}), (b) meridional eddy heat flux (shading; K m s^{-1}) and zonal wind (contours; m s^{-1}) at 850 hPa, and (c) standard deviation of 2–7-day band-pass-filtered meridional wind (shading; m s^{-1}) and zonal wind (contours; m s^{-1}) at 300 hPa. Solid (dashed) contours indicate positive (negative) differences, with contour levels at ±1, ±2, ±3, and ±4 m s^{-1} for panels (a) and (b), and ±2, ±4, and ±6 m s^{-1} for panel (c). Hatching indicates regions where the shaded differences are not statistically significant at the 99% confidence level, based on a Student's *t*-test.

https://doi.org/10.5194/egusphere-2026-3834
Preprint. Discussion started: 8 July 2026

In both climate states, robust upward wave activity originated from the strongly baroclinic lower troposphere near 55°S (Figs. 7a and 7b). As these waves ascended into the upper troposphere, the EP flux diminished with equatorward veering, leading to widespread convergence. This convergence signifies wave breaking, acting as a momentum sink that decelerates the upper-level westerly mean flow. Crucially, this wave-breaking process does not merely reduce the upper-level westerly wind strength; it effectively draws upper-tropospheric momentum downward, where it dynamically balances surface friction to maintain the surface westerlies (Vallis, 2017).

Reflecting the enhanced baroclinicity driven by LGM sea ice, anomalous upward EP flux vectors emerged from the lower troposphere and propagated into the upper troposphere (Fig. 7c). This strong upward wave propagation leaves behind a robust EP-flux divergence in the lower troposphere along the Antarctic margin, which dynamically accelerates the near-surface westerlies. Spectral decomposition confirms that this vigorous vertical wave propagation was predominantly driven by synoptic-scale eddies (zonal wavenumbers k = 4-9; Fig. S1), which are the primary modes generated by enhanced baroclinic instability. As these anomalous synoptic eddies strongly converge near the tropopause (Edmon et al., 1980), they act as a momentum sink that drives a downward transfer of westerly momentum. Consistent with the intensified poleward heat transport, this dynamic sequence illustrates how the LGM sea ice generated substantially greater wave energy aloft, ultimately enhancing the surface westerlies.

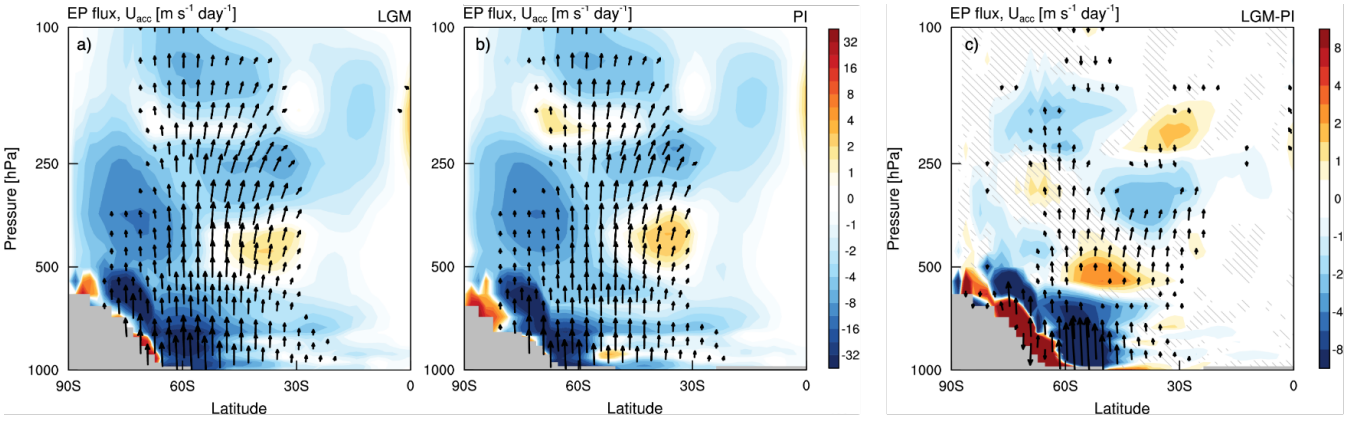

Figure 7: EP flux (vectors) and zonal wind acceleration (shading; m s^{-1} day^{-1}) during austral winter (JJA) for (a) LGM, (b) PI, and (c) the difference (LGM minus PI). Positive (negative) shading indicates westerly (easterly) acceleration driven by EP flux divergence (convergence). Vectors are scaled by $e^{z/H}$ for visual clarity. Note that the vector and shading scales in panel (c) are reduced by a factor of 4 compared to panels (a) and (b). Hatching indicates regions where the shaded differences are not statistically significant at the 99% confidence level based on a Student's *t*-test.

The Eulerian framework also provides direct insight into how the mean meridional circulation adjusts to maintain the momentum balance. In the mid-latitudes, circulation is dominated by thermally indirect Ferrel cells, characterized by sinking

https://doi.org/10.5194/egusphere-2026-3834
Preprint. Discussion started: 8 July 2026

motion in the subtropics and rising motion in the subpolar region (Figs. 8a and 8b). A crucial feature of this cell is its near-surface poleward flow. As air parcels move poleward, the Coriolis force deflects them eastward, generating a westerly acceleration at mid-latitudes.

Under LGM boundary conditions, this dynamic response was significantly intensified within the Ferrel cell (Fig. 8c). Driven by the increased lower-tropospheric baroclinicity, enhanced synoptic eddies produced stronger eddy heat and momentum fluxes. To maintain thermal wind balance against this vigorous eddy forcing, an anomalous thermally indirect circulation was generated, manifesting as an anomalous clockwise mass stream function centered near 50°S. This intensified Ferrel cell induced an anomalous poleward flow in the lower troposphere, generating additional surface westerly acceleration via the Coriolis effect. Consequently, the SHW was effectively intensified and shifted poleward through eddy-driven secondary circulation.

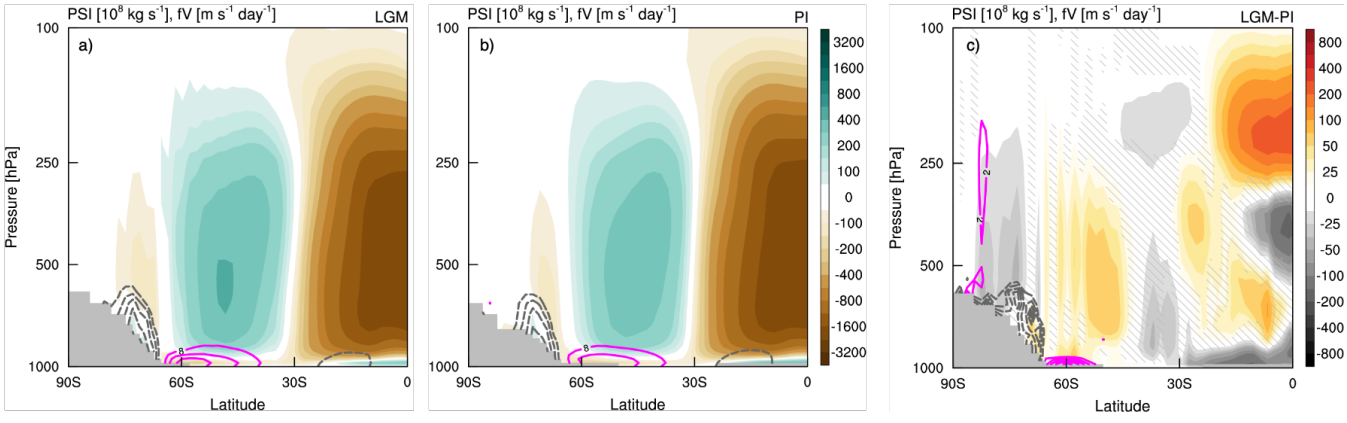

Figure 8: Zonal-mean mass streamfunction and the Coriolis acceleration term, averaged over austral winter (JJA). Mass streamfunction (shading; 10^8 kg s^{-1}) and the zonal wind acceleration induced by the Coriolis force (contours; m s^{-1} day^{-1}) for (a) LGM, (b) PI, and (c) the difference (LGM minus PI). Positive (negative) shading indicates clockwise (counterclockwise) circulation. Solid (dashed) contours indicate westerly (easterly) acceleration, with contour levels at ±8, ±16, ±24, and ±32 m s^{-1} day^{-1} for panels (a) and (b). Note that the contour intervals and shading scales in (c) are reduced by a factor of 4 compared to panels (a) and (b). Hatching indicates regions where the shaded differences are not statistically significant at the 99% confidence level, based on a Student's *t*-test.

3.3 Sensitivity of the Southern Hemisphere westerlies to sea-ice expansion

Previous studies have demonstrated that sea-ice expansion suppresses the upward heat flux, contributing to near-surface atmospheric cooling (e.g., Alexander et al., 2004). While this localized thermodynamic response is evident in our LGM simulation, a quantitative assessment is required to isolate how Antarctic sea-ice expansion ultimately drives the SHW shift. To this end, we analyzed the area-averaged surface heat fluxes and the 2 m temperatures across the PI, ICE sensitivity, and

https://doi.org/10.5194/egusphere-2026-3834
Preprint. Discussion started: 8 July 2026

345 LGM experiments (Fig. 9). For a direct thermodynamic comparison, the Southern Ocean was partitioned at the LGM sea-ice edge (~55°S) into a northern open-ocean band (area 1; 45°S-55°S) and a southern ice-covered band (area 2; 55°S-65°S).

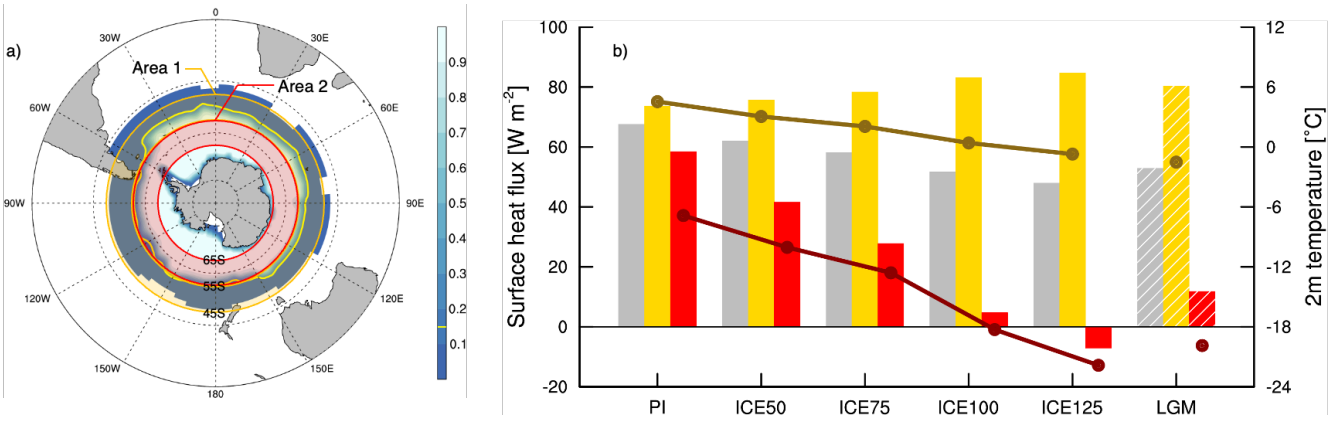

Figure 9: Analysis domains and surface boundary conditions. (a) Map illustrating two key analysis regions overlaid on the sea-ice 350 **concentration field. Area 1 (45°S-55°S, orange) and Area 2 (55°S-65°S, red) represent the open ocean and sea ice zones, respectively. The yellow contour marks the sea ice edge (threshold: 0.15). (b) Surface upward heat flux (bars; W m^{-2}) and 2-meter temperature (lines; °C) averaged over Area 1 and Area 2 for each simulation. Yellow and red colors correspond to Area 1 and Area 2, respectively. Gray bars show the average over the combined region. Hatched bars indicate the LGM experiment.**

355 Between the PI and LGM simulations, the thermodynamic impact of sea-ice forcing exhibited a stark meridional contrast. In the ice-covered Area 2, the expanded LGM sea-ice physically blocked heat transfer, drastically suppressing the upward heat flux (from 58.4 W m^{-2} to 11.8 W m^{-2}) and driving a severe surface temperature drop (−6.9 °C to −19.9 °C). Conversely, the open-ocean Area 1 remained largely ice-free and continued to act as an active heat source, maintaining a robust surface heat release (from 73.7 W m^{-2} to 80.4 W m^{-2}) that effectively buffered the regional cooling (4.5 °C to −1.5 °C). Consequently, this 360 differential cooling across the sea-ice edge directly amplified the lower-tropospheric meridional temperature gradient.

The ICE sensitivity experiments confirmed that this thermodynamic contrast scales directly with sea-ice expansion. As the prescribed sea-ice concentration increased across the experiments, the differential heat release between the ice-covered and open-ocean regions systematically amplified. The meridional temperature gradients across the sea-ice edge intensified in 365 proportion to the sea-ice expansion, thereby directly modulating the SHW intensity.

To quantify the jet's sensitivity to sea-ice expansion, we evaluated the statistical relationship between the lower-tropospheric SHW core and the sea ice edge—defined by 0.7 concentration threshold to capture significant ice expansion (Fig. 10a). Between the PI (ice edge: 63.8°S; jet: 52.7°S) and the LGM states (ice edge: 56.5°S; jet: 54.6°S), the SHW exhibited a net 370 poleward shift of 1.9°. However, this net displacement reflected the competing influence of two opposing drivers: sea-ice

https://doi.org/10.5194/egusphere-2026-3834
Preprint. Discussion started: 8 July 2026

expansion promoting a poleward shift, and global atmospheric cooling inducing an equatorward shift. The ICE100 experiment, which isolates the sea-ice effect, produced a stronger poleward SHW displacement of 2.7° (reaching 55.4°S).

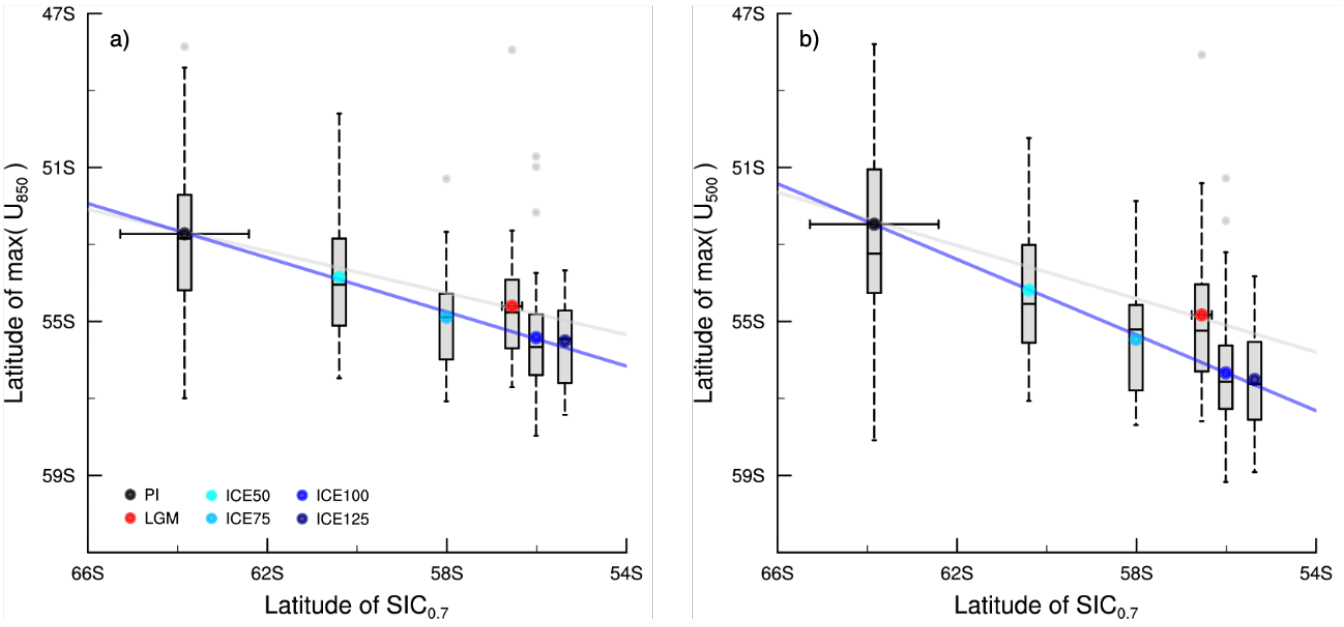

Figure 10: Relationship between the sea-ice edge latitude and the lower-tropospheric jet latitude during austral winter (JJA). The x-axis represents the latitude of the sea-ice edge defined by a sea-ice concentration of 0.7 ($SIC_{0.7}$), and the y-axis denotes the latitude of the maximum zonal-mean zonal wind at (a) 850 hPa and (b) 500 hPa. Box-and-whisker plots show the interannual variability for each simulation: boxes (interquartile range; IQR), horizontal lines (median), whiskers (data within 1.5×IQR), and gray dots (outliers). Colored circles indicate climatological means, with horizontal error bars representing ±1 standard deviation of the sea-ice edge latitude. The blue solid lines indicate the linear trend derived from the PI and ICE simulations; the gray solid line indicates the trend from the PI and LGM simulations.

The difference between this isolated sea ice effect (2.7° poleward) and the LGM state (1.9° poleward) highlights the opposing role of the tropical atmosphere. The cold LGM tropics contracted the Hadley cells, pulling the SHW equatorward by ~0.8° and partially offsetting the sea-ice-driven shift. Nevertheless, the poleward forcing from sea-ice expansion remained quantitatively dominant. Furthermore, the lower-tropospheric jet exhibited a significant linear response across the sensitivity experiments (PI to ICE125), shifting poleward by approximately 0.35° for every 1° of equatorward sea-ice expansion (slope ≈ –0.35). This linear dependence supports the multi-model findings of Sime et al. (2016).

This linear relationship extended to the mid-tropospheric SHW at 500 hPa (Fig. 10b). Notably, the SHW response to the sea ice forcing was even more pronounced aloft, exhibiting a steeper slope of approximately -0.49. This amplified upper-level response is dynamically consistent with the thermal wind balance. The steepened lower-tropospheric temperature gradient driven by the expanded sea ice integrated with height, resulting in stronger westerly acceleration and a more distinct poleward

https://doi.org/10.5194/egusphere-2026-3834
Preprint. Discussion started: 8 July 2026

shift. These robust trends across the troposphere effectively encapsulate how the poleward shift of the SHW is dynamically coupled with near-surface Antarctic cooling driven by sea-ice expansion. Consequently, these results confirm that Antarctic sea ice is an important driver of LGM circulation changes.

4 Summary and conclusion

This study identifies the SHW response by elucidating the dynamic interaction between Antarctic sea ice and atmospheric circulation during the LGM. Our findings reveal that the extensive expansion of Antarctic sea ice serves as a critical variable that sharply steepens the meridional temperature gradient in the lower troposphere. Through the thermal wind relationship, this enhanced temperature gradient directly drives a poleward intensification of the upper-tropospheric westerlies. Concurrently, the steepened gradient amplifies atmospheric baroclinicity, thereby invigorating eddy activity. The subsequent downward transfer of eddy momentum effectively translates this upper-level momentum to the surface, leading to a robust poleward shift and intensification of the surface SHW. This sequence of physical causality suggests that Antarctic sea ice acts as the primary forcing that initiates the near-surface thermal anomalies and reorganizes the atmospheric circulation structure.

Quantitative analysis demonstrates that the effect of high-latitude sea-ice expansion overwhelmingly dominates over tropical cooling in determining SHW variability. This mechanistic hierarchy provides a physical basis for explaining the profound inter-model spread in SHW simulations across PMIP models, which ultimately stems from disparities in sea-ice representation. Figure 11 schematically summarizes these competing dynamic mechanisms. While upper-tropospheric tropical cooling exerts an equatorward pull on the broader SHW system, it is ultimately overpowered by sea-ice-driven surface cooling. Therefore, we conclude that the poleward intensification of the LGM westerlies is not a passive response to uniform global cooling, but a dynamical product governed by Antarctic sea-ice expansion, which dictates the net atmospheric circulation through the thermal wind balance and eddy activity.

https://doi.org/10.5194/egusphere-2026-3834
Preprint. Discussion started: 8 July 2026

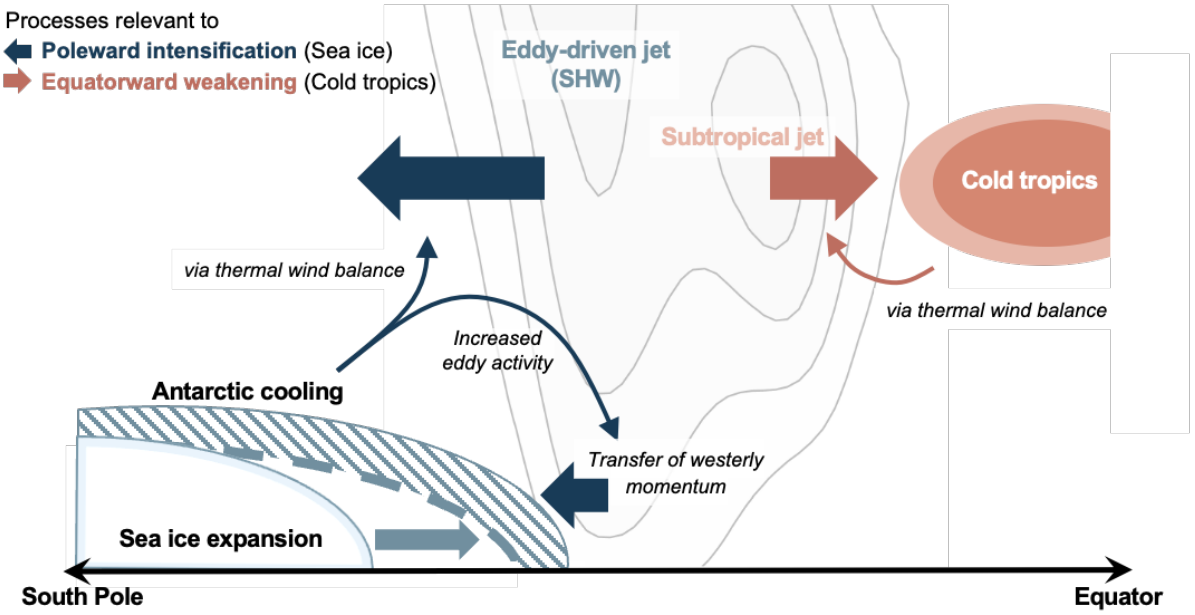

Figure 11: Schematic diagram summarizing the opposing influences of Antarctic near-surface cooling and upper-tropospheric tropical cooling on the SHW. Navy arrows indicate the dynamical processes driving the poleward intensification of the SHW associated with expanded sea ice, while orange arrows represent the processes driving the equatorward weakening associated with upper-tropospheric tropical cooling.

5 Discussion

While our simulations demonstrate a robust poleward intensification of the SHW driven by Antarctic sea-ice (Fig. 2d), we note that this result contrasts with several proxy-based reconstructions suggesting a 3°–5° equatorward displacement of the westerlies during the LGM (Kohfeld et al., 2013). This apparent discrepancy can be reconciled through the competing dynamic mechanisms identified in this study (Fig. 11). As demonstrated by the ICE sensitivity experiments, the net SHW response is highly sensitive to the Antarctic surface cooling associated with sea-ice. If the LGM sea-ice expansion and the resulting Antarctic cooling were less intensified, the equatorward pull exerted by tropical upper-tropospheric cooling would have dominated the net circulation change, resulting in a circulation state more consistent with the equatorward shift inferred from proxy records. Regarding wind intensity, our model physically supports a strengthening of the surface SHW, dynamically sustained by enhanced eddy activity near the ice margin. This aligns with most proxy records supporting stronger glacial winds (Kohfeld et al., 2013). However, some paleoclimate data can also be interpreted as a weakening of the winds. Notably, a recent reconstruction inferred a 25% weakening of the westerlies during the LGM relative to the mid-Holocene (Gray et al., 2023). Our mechanistic framework implies that regardless of the overall latitudinal position, the surface westerlies must have locally intensified where the sea-ice-driven temperature gradient was steepest, emphasizing the necessity of accounting for regional difference in proxy interpretations.

https://doi.org/10.5194/egusphere-2026-3834
Preprint. Discussion started: 8 July 2026

The interplay between tropical and high-latitude thermal drivers provides a valuable paleo-perspective on the 'tug-of-war' framework (e.g, Deser et al., 2015; Screen et al., 2018). While modern anthropogenic warming involves a competition between tropical warming and polar sea-ice loss, the LGM acts as an opposite counterpart where widespread tropical cooling competes against Antarctic sea-ice expansion. In our simulation, the extreme meridional temperature gradient driven by this sea-ice expansion dominates the tug of war, amplifying eddy activity and leading to a poleward intensification of the SHW. In the context of modern climate experiments, Screen et al. (2022) point out that climate models with stronger eddy feedback simulate farther jet shifts in response to sea-ice changes. Consistent with this, our results imply that our model operates with a strong eddy feedback, which drives an additional response of the SHW. As discussed earlier, the model-proxy discrepancy suggests that the prescribed sea-ice forcing may be overestimated, and that efficient eddy feedback amplified this excessively dominant poleward driver.

Although this study primarily focuses on the Southern Hemisphere winter, the dynamic coupling between sea ice and the SHW exhibits strong seasonality, driven by highly seasonal surface heat fluxes (Fig. S2; Ayres et al., 2022). The magnitude of this wintertime forcing depends on the winter sea-ice coverage, which is inherently preconditioned by the remaining sea ice during the preceding seasons. During austral spring and summer, strong incoming solar radiation maximizes the surface albedo feedback (Hall, 2004). Variations in this feedback mechanism could modulate the summer sea-ice concentration and, by extension, the winter coverage, eventually contributing to the inter-model spread. Notably, these differences can be amplified by cloud-radiation biases, which further alter the net albedo and widen the spread across climate models (e.g., Ceppi et al., 2012; Sherriff-Tadano et al., 2023). This seasonal memory effect offers a plausible reason why models exhibiting poleward intensification of the SHW are typically accompanied by extensive Antarctic sea ice cover. For instance, the CCSM4 family (e.g., CCSM4 in PMIP3 and UoT-CCSM4 in PMIP4) simulates the most extensive sea ice across both summer and winter and significantly overestimates its coverage compared with LGM proxy reconstructions (Green et al., 2022). This leads to excessive Antarctic cooling, which drives robust poleward intensification of the SHW. Conversely, models with the least sea ice, such as GISS-E2-R in PMIP3, exhibit equatorward weakening of the SHW (Sime et al., 2016).

The SHW variability remains a significant challenge in understanding the global carbon cycle, an intricate system governed by multiple interconnected processes (Gottschalk et al., 2019). The strong SHW is generally known to drive deep-water upwelling over the open ocean area through Ekman pumping, facilitating CO_2 outgassing. However, the simultaneous expansion of Antarctic sea ice and associated poleward intensification of SHW could offset this CO_2 ventilation. Extensive sea-ice cover acts as a physical barrier that restricts air-sea gas exchange (Stephens and Keeling, 2000). Concurrently, enhanced sea-ice production intensifies brine rejection over the continental shelves. While this localized process induces strong surface sinking, the resulting highly saline water ultimately cascades to the abyss, substantially expanding the dense Antarctic Bottom Water (AABW) mass (Bouttes et al., 2010; Ferrari et al., 2014; Lhardy et al., 2021). The accumulation of this dense water at the ocean floor steepens the vertical density gradient between the AABW and North Atlantic deep water, thereby restricting

https://doi.org/10.5194/egusphere-2026-3834
Preprint. Discussion started: 8 July 2026

vertical mixing and preventing carbon-rich deep waters from upwelling (Nadeau et al., 2019). Together, these physical mechanisms, effectively isolate carbon in the deep ocean, accounting for a substantial atmospheric CO_2 drawdown of approximately 40 ppm (Marzocchi and Jansen, 2019; Stein et al., 2020). Previous studies suggest that this carbon change was a result of the expansion of Antarctic sea-ice and accompanying changes in the overturning circulation along with ocean biological factors (e.g., Kohfeld and Chase, 2017; Omta et al., 2024). Since these ocean dynamics and interactions with the atmosphere and sea ice amplify LGM cooling and sustain massive sea-ice expansion (Zhu and Poulsen, 2021), accurately simulating such combined processes remains a crucial step forward for improving future paleoclimate models.

Code and data availability

The Community Earth System Model version 1.2 (CESM 1.2) source code is publicly available through the National Center for Atmospheric Research (NCAR) repository (https://www.cesm.ucar.edu). The processed datasets and specific model configuration files used to reproduce the findings and figures of this study are available from the corresponding author upon request.

Supplement link

The link to the supplement will be included by Copernicus, if applicable.

Author contributions

JWK, SYJ, and SJK conceptualized the study. SYJ developed the methodology and performed the model simulations. HGK and JWK conducted the formal data analysis. SJK provided overall project administration. JWK supervised the research and acquired the financial support. HGK wrote the initial draft of the manuscript and created the visualizations. JWK, SYJ, SJK, and DS contributed to the critical review and editing of the text. All authors discussed the results and approved the final manuscript.

https://doi.org/10.5194/egusphere-2026-3834
Preprint. Discussion started: 8 July 2026

Competing interests

The authors declare that they have no conflict of interest.

Disclaimer

Copernicus Publications adds a standard disclaimer: "Copernicus Publications remains neutral with regard to jurisdictional claims made in the text, published maps, institutional affiliations, or any other geographical representation in this paper. While Copernicus Publications makes every effort to include appropriate place names, the final responsibility lies with the authors. Views expressed in the text are those of the authors and do not necessarily reflect the views of the publisher."

Financial support

This research was supported by Korea Institute of Marine Science & Technology Promotion (KIMST) funded by the Ministry of Oceans and Fisheries (RS-2026-25543619) and the Specialized University Program for Confluence Analysis of Weather and Climate Data of the Korea Meteorological Institute (KMI) funded by the Korean government (KMA).

References

Abe-Ouchi, A., Saito, F., Kageyama, M., Braconnot, P., Harrison, S. P., Lambeck, K., Otto-Bliesner, B. L., Peltier, W. R., Tarasov, L., Peterschmitt, J.-Y., and Takahashi, K.: Ice-sheet configuration in the CMIP5/PMIP3 Last Glacial Maximum experiments, Geosci. Model Dev., 8, 3621–3637, https://doi.org/10.5194/gmd-8-3621-2015, 2015.

Abram, N. J., Mulvaney, R., Vimeux, F., Phipps, S. J., Turner, J., and England, M. H.: Evolution of the Southern Annular Mode during the past millennium, Nature Clim Change, 4, 564–569, https://doi.org/10.1038/nclimate2235, 2014.

https://doi.org/10.5194/egusphere-2026-3834
Preprint. Discussion started: 8 July 2026

Alexander, M. A., Bhatt, U. S., Walsh, J. E., Timlin, M. S., Miller, J. S., and Scott, J. D.: The Atmospheric Response to Realistic Arctic Sea Ice Anomalies in an AGCM during Winter, J. Climate, 17, 890–905, https://doi.org/10.1175/1520-0442(2004)017%3C0890:TARTRA%3E2.0.CO;2, 2004.

Anderson, R. F., Ali, S., Bradtmiller, L. I., Nielsen, S. H. H., Fleisher, M. Q., Anderson, B. E., and Burckle, L. H.: Wind-Driven Upwelling in the Southern Ocean and the Deglacial Rise in Atmospheric CO_2, Science, 323, 1443–1448, https://doi.org/10.1126/science.1167441, 2009.

Andrews, D. G., Holton, J. R., and Leovy, C. B.: Middle Atmosphere Dynamics, International Geophysics Series, Vol. 40, Academic Press, San Diego, CA, 489 pp., 1987.

Ayres, H. C., Screen, J. A., Blockley, E. W., and Bracegirdle, T. J.: The Coupled Atmosphere–Ocean Response to Antarctic Sea Ice Loss, Journal of Climate, 35, 4665–4685, https://doi.org/10.1175/JCLI-D-21-0918.1, 2022.

Bader, J., Flügge, M., Kvamstø, N. G., Mesquita, M. D. S., and Voigt, A.: Atmospheric winter response to a projected future Antarctic sea-ice reduction: a dynamical analysis, Clim Dyn, 40, 2707–2718, https://doi.org/10.1007/s00382-012-1507-9, 2013.

Banerjee, A., Yeung, L. Y., Murray, L. T., Tie, X., Tierney, J. E., and Legrande, A. N.: Clumped-Isotope Constraint on Upper-Tropospheric Cooling During the Last Glacial Maximum, AGU Advances, 3, e2022AV000688, https://doi.org/10.1029/2022AV000688, 2022.

Barnes, E. A. and Polvani, L.: Response of the Midlatitude Jets, and of Their Variability, to Increased Greenhouse Gases in the CMIP5 Models, Journal of Climate, 26, 7117–7135, https://doi.org/10.1175/JCLI-D-12-00536.1, 2013.

Berger, AndréL.: Long-Term Variations of Daily Insolation and Quaternary Climatic Changes, J. Atmos. Sci., 35, 2362–2367, https://doi.org/10.1175/1520-0469(1978)035%3C2362:LTVODI%3E2.0.CO;2, 1978.

Bouttes, N., Paillard, D., and Roche, D. M.: Impact of brine-induced stratification on the glacial carbon cycle, Clim. Past, 6, 575–589, https://doi.org/10.5194/cp-6-575-2010, 2010.

https://doi.org/10.5194/egusphere-2026-3834
Preprint. Discussion started: 8 July 2026

Braconnot, P., Harrison, S. P., Kageyama, M., Bartlein, P. J., Masson-Delmotte, V., Abe-Ouchi, A., Otto-Bliesner, B., and Zhao, Y.: Evaluation of climate models using palaeoclimatic data, Nature Clim Change, 2, 417–424, https://doi.org/10.1038/nclimate1456, 2012.

Brayshaw, D. J., Hoskins, B., and Blackburn, M.: The Storm-Track Response to Idealized SST Perturbations in an Aquaplanet GCM, Journal of the Atmospheric Sciences, 65, 2842–2860, https://doi.org/10.1175/2008JAS2657.1, 2008.

Buizert, C., Fudge, T. J., Roberts, W. H. G., Steig, E. J., Sherriff-Tadano, S., Ritz, C., Lefebvre, E., Edwards, J., Kawamura, K., Oyabu, I., Motoyama, H., Kahle, E. C., Jones, T. R., Abe-Ouchi, A., Obase, T., Martin, C., Corr, H., Severinghaus, J. P., Beaudette, R., Epifanio, J. A., Brook, E. J., Martin, K., Chappellaz, J., Aoki, S., Nakazawa, T., Sowers, T. A., Alley, R. B., Ahn, J., Sigl, M., Severi, M., Dunbar, N. W., Svensson, A., Fegyveresi, J. M., He, C., Liu, Z., Zhu, J., Otto-Bliesner, B. L., Lipenkov, V. Y., Kageyama, M., and Schwander, J.: Antarctic surface temperature and elevation during the Last Glacial Maximum, Science, 372, 1097–1101, https://doi.org/10.1126/science.abd2897, 2021.

Ceppi, P., Hwang, Y., Frierson, D. M. W., and Hartmann, D. L.: Southern Hemisphere jet latitude biases in CMIP5 models linked to shortwave cloud forcing, Geophysical Research Letters, 39, 2012GL053115, https://doi.org/10.1029/2012GL053115, 2012.

Chang, E. K. M., Lee, S., and Swanson, K. L.: Storm Track Dynamics, J. Climate, 15, 2163–2183, https://doi.org/10.1175/1520-0442(2002)015%3C02163:STD%3E2.0.CO;2, 2002.

Chase, Z., Kohfeld, K. E., Leventer, A., Lund, D., Crosta, X., Menviel, L., Bostock, H. C., Chadwick, M., Jaccard, S. L., Jones, J., Marzocchi, A., Meissner, K. J., Sikes, E., Sime, L. C., and Skinner, L.: The role of Antarctic sea ice in the Earth system: Perspectives informed by 130,000 years of sea ice records, https://doi.org/10.5194/egusphere-2025-3504, 1 August 2025.

Chavaillaz, Y., Codron, F., and Kageyama, M.: Southern westerlies in LGM and future (RCP4.5) climates, Clim. Past, 9, 517–524, https://doi.org/10.5194/cp-9-517-2013, 2013.

Chen, G., Plumb, R. A., and Lu, J.: Sensitivities of zonal mean atmospheric circulation to SST warming in an aqua-planet model, Geophysical Research Letters, 37, 2010GL043473, https://doi.org/10.1029/2010GL043473, 2010.

Chen, H., Xu, Z., Bayon, G., Fan, Q., Pogge Von Strandmann, P. A. E., Wang, W., Sun, T., and Li, T.: Meridional Shifts of the Southern Hemisphere Westerlies During the Early Cenozoic, Geophysical Research Letters, 51, e2024GL110182, https://doi.org/10.1029/2024GL110182, 2024.

https://doi.org/10.5194/egusphere-2026-3834
Preprint. Discussion started: 8 July 2026

Dällenbach, A., Blunier, T., Flückiger, J., Stauffer, B., Chappellaz, J., and Raynaud, D.: Changes in the atmospheric CH_4 gradient between Greenland and Antarctica during the Last Glacial and the transition to the Holocene, Geophysical Research Letters, 27, 1005–1008, https://doi.org/10.1029/1999GL010873, 2000.

Deng, K., Azorin-Molina, C., Yang, S., Hu, C., Zhang, G., Minola, L., and Chen, D.: Changes of Southern Hemisphere westerlies in the future warming climate, Atmospheric Research, 270, 106040, https://doi.org/10.1016/j.atmosres.2022.106040, 2022.

Deser, C., Tomas, R. A., and Sun, L.: The Role of Ocean–Atmosphere Coupling in the Zonal-Mean Atmospheric Response to Arctic Sea Ice Loss, Journal of Climate, 28, 2168–2186, https://doi.org/10.1175/JCLI-D-14-00325.1, 2015.

Dixon, D. A., Mayewski, P. A., Goodwin, I. D., Marshall, G. J., Freeman, R., Maasch, K. A., and Sneed, S. B.: An ice-core proxy for northerly air mass incursions into West Antarctica, Intl Journal of Climatology, 32, 1455–1465, https://doi.org/10.1002/joc.2371, 2011.

Du, Y., Brown, J. R., and Sniderman, J. M. K.: Last Glacial Maximum climate and atmospheric circulation over the Australian region from climate models, Clim. Past, 20, 393–413, https://doi.org/10.5194/cp-20-393-2024, 2024.

Edmon, H. J., Hoskins, B. J., and McIntyre, M. E.: Eliassen-Palm Cross Sections for the Troposphere, J. Atmos. Sci., 37, 2600–2616, https://doi.org/10.1175/1520-0469(1980)037%3C2600:EPCSFT%3E2.0.CO;2, 1980.

Ferrari, R., Jansen, M. F., Adkins, J. F., Burke, A., Stewart, A. L., and Thompson, A. F.: Antarctic sea ice control on ocean circulation in present and glacial climates, Proc. Natl. Acad. Sci. U.S.A., 111, 8753–8758, https://doi.org/10.1073/pnas.1323922111, 2014.

Flückiger, J., Dällenbach, A., Blunier, T., Stauffer, B., Stocker, T. F., Raynaud, D., and Barnola, J.-M.: Variations in Atmospheric N_2O Concentration During Abrupt Climatic Changes, Science, 285, 227–230, https://doi.org/10.1126/science.285.5425.227, 1999.

Fogt, R. L. and Marshall, G. J.: The Southern Annular Mode: Variability, trends, and climate impacts across the Southern Hemisphere, WIREs Climate Change, 11, e652, https://doi.org/10.1002/wcc.652, 2020.

https://doi.org/10.5194/egusphere-2026-3834
Preprint. Discussion started: 8 July 2026

Fu, Q., Johanson, C. M., Wallace, J. M., and Reichler, T.: Enhanced Mid-Latitude Tropospheric Warming in Satellite Measurements, Science, 312, 1179–1179, https://doi.org/10.1126/science.1125566, 2006.

Gottschalk, J., Battaglia, G., Fischer, H., Frölicher, T. L., Jaccard, S. L., Jeltsch-Thömmes, A., Joos, F., Köhler, P., Meissner, K. J., Menviel, L., Nehrbass-Ahles, C., Schmitt, J., Schmittner, A., Skinner, L. C., and Stocker, T. F.: Mechanisms of millennial-scale atmospheric CO2 change in numerical model simulations, Quaternary Science Reviews, 220, 30–74, https://doi.org/10.1016/j.quascirev.2019.05.013, 2019.

Goyal, R., Sen Gupta, A., Jucker, M., and England, M. H.: Historical and Projected Changes in the Southern Hemisphere Surface Westerlies, Geophysical Research Letters, 48, e2020GL090849, https://doi.org/10.1029/2020GL090849, 2021.

Gray, W. R., De Lavergne, C., Jnglin Wills, R. C., Menviel, L., Spence, P., Holzer, M., Kageyama, M., and Michel, E.: Poleward Shift in the Southern Hemisphere Westerly Winds Synchronous With the Deglacial Rise in CO_2, Paleoceanog and Paleoclimatol, 38, e2023PA004666, https://doi.org/10.1029/2023PA004666, 2023.

Green, R. A., Menviel, L., Meissner, K. J., Crosta, X., Chandan, D., Lohmann, G., Peltier, W. R., Shi, X., and Zhu, J.: Evaluating seasonal sea-ice cover over the Southern Ocean at the Last Glacial Maximum, Clim. Past, 18, 845–862, https://doi.org/10.5194/cp-18-845-2022, 2022.

Hall, A.: The Role of Surface Albedo Feedback in Climate, J. Climate, 17, 1550–1568, https://doi.org/10.1175/1520-0442(2004)017%3C1550:TROSAF%3E2.0.CO;2, 2004.

Hall, A. and Visbeck, M.: Synchronous Variability in the Southern Hemisphere Atmosphere, Sea Ice, and Ocean Resulting from the Annular Mode*, J. Climate, 15, 3043–3057, https://doi.org/10.1175/1520-0442(2002)015%3C3043:SVITSH%3E2.0.CO;2, 2002.

Harrison, S. P., Bartlein, P. J., Izumi, K., Li, G., Annan, J., Hargreaves, J., Braconnot, P., and Kageyama, M.: Evaluation of CMIP5 palaeo-simulations to improve climate projections, Nature Clim Change, 5, 735–743, https://doi.org/10.1038/nclimate2649, 2015.

Hodgson, D. A. and Sime, L. C.: Southern westerlies and CO2, Nature Geosci, 3, 666–667, https://doi.org/10.1038/ngeo970, 2010.

https://doi.org/10.5194/egusphere-2026-3834
Preprint. Discussion started: 8 July 2026

Hogg, A. McC., Meredith, M. P., Chambers, D. P., Abrahamsen, E. P., Hughes, C. W., and Morrison, A. K.: Recent trends in the S outhern O cean eddy field, JGR Oceans, 120, 257–267, https://doi.org/10.1002/2014JC010470, 2015.

Holton, J. R.: An Introduction to Dynamic Meteorology, 4th edn., Elsevier Academic Press, Burlington, MA, 535 pp., 2004.

Hunke, E. C. and Lipscomb, W. H.: CICE: the Los Alamos Sea Ice Model Documentation and Software User's Manual Version 4.1, Los Alamos National Laboratory Tech. Rep. LA-CC-06-012, 2010.

Hurrell, J. W., Holland, M. M., Gent, P. R., Ghan, S., Kay, J. E., Kushner, P. J., Lamarque, J.-F., Large, W. G., Lawrence, D., Lindsay, K., Lipscomb, W. H., Long, M. C., Mahowald, N., Marsh, D. R., Neale, R. B., Rasch, P., Vavrus, S., Vertenstein, M., Bader, D., Collins, W. D., Hack, J. J., Kiehl, J., and Marshall, S.: The Community Earth System Model: A Framework for Collaborative Research, Bull. Amer. Meteor. Soc., 94, 1339–1360, https://doi.org/10.1175/BAMS-D-12-00121.1, 2013.

Ivanciu, I., Matthes, K., Biastoch, A., Wahl, S., and Harlaß, J.: Twenty-first-century Southern Hemisphere impacts of ozone recovery and climate change from the stratosphere to the ocean, Weather Clim. Dynam., 3, 139–171, https://doi.org/10.5194/wcd-3-139-2022, 2022.

Jucker, M.: Scaling of ELIASSEN-PALM flux vectors, Atmospheric Science Letters, 22, https://doi.org/10.1002/asl.1020, 2021.
Kageyama, M., Braconnot, P., Chiessi, C. M., Rehfeld, K., Ait Brahim, Y., Dütsch, M., Gwinneth, B., Hou, A., Loutre, M.-F., Hendrizan, M., Meissner, K., Mongwe, P., Otto-Bliesner, B., Pezzi, L. P., Rovere, A., Seltzer, A., Sime, L., and Zhu, J.: Lessons from paleoclimates for recent and future climate change: opportunities and insights, Front. Clim., 6, 1511997, https://doi.org/10.3389/fclim.2024.1511997, 2024.

Kidston, J., Taschetto, A. S., Thompson, D. W. J., and England, M. H.: The influence of Southern Hemisphere sea-ice extent on the latitude of the mid-latitude jet stream, Geophysical Research Letters, 38, 2011GL048056, https://doi.org/10.1029/2011GL048056, 2011.

Kim, S.-J. and Lee, B. Y.: Westerly Winds in the Southern Ocean During the Last Glacial Maximum Simulated in CCM3, Ocean and Polar Research, 32, 297–304, https://doi.org/10.4217/OPR.2009.31.4.297, 2009.

Kim, S.-J., Flato, G. M., Boer, G. J., and McFarlane, N. A.: A coupled climate model simulation of the Last Glacial Maximum, Part 1: transient multi-decadal response, Climate Dynamics, 19, 515–537, https://doi.org/10.1007/s00382-002-0243-y, 2002.

https://doi.org/10.5194/egusphere-2026-3834
Preprint. Discussion started: 8 July 2026

Kim, S.-J., Jun, S.-Y., and Kim, B.-M.: Sensitivity of southern hemisphere westerly wind to boundary conditions for the last glacial maximum, Quaternary International, 459, 165–174, https://doi.org/10.1016/j.quaint.2017.04.001, 2017.

Kim, S.-Y. and Son, S.-W.: Breakdown of the Linear Relationship between the Southern Hemisphere Hadley Cell Edge and Jet Latitude Changes in the Last Glacial Maximum, Journal of Climate, 33, 5713–5725, https://doi.org/10.1175/JCLI-D-19-0531.1, 2020.

Kim, S.-Y. and Son, S.-W.: Opposing Shifts of the Hadley Cell Edge and Eddy-Driven Jet Latitude in the Last Glacial Maximum: A Parameter Sweep Study Using a Dynamical Core GCM, Journal of Climate, 36, 885–898, https://doi.org/10.1175/JCLI-D-21-0989.1, 2023.

Kohfeld, K. E. and Chase, Z.: Temporal evolution of mechanisms controlling ocean carbon uptake during the last glacial cycle, Earth and Planetary Science Letters, 472, 206–215, https://doi.org/10.1016/j.epsl.2017.05.015, 2017.

Kohfeld, K. E., Graham, R. M., De Boer, A. M., Sime, L. C., Wolff, E. W., Le Quéré, C., and Bopp, L.: Southern Hemisphere westerly wind changes during the Last Glacial Maximum: paleo-data synthesis, Quaternary Science Reviews, 68, 76–95, https://doi.org/10.1016/j.quascirev.2013.01.017, 2013.

Lamy, F., Kilian, R., Arz, H. W., Francois, J.-P., Kaiser, J., Prange, M., and Steinke, T.: Holocene changes in the position and intensity of the southern westerly wind belt, Nature Geosci, 3, 695–699, https://doi.org/10.1038/ngeo959, 2010.

Lamy, F., Gersonde, R., Winckler, G., Esper, O., Jaeschke, A., Kuhn, G., Ullermann, J., Martinez-Garcia, A., Lambert, F., and Kilian, R.: Increased Dust Deposition in the Pacific Southern Ocean During Glacial Periods, Science, 343, 403–407, https://doi.org/10.1126/science.1245424, 2014.

Landrum, L. L. and Holland, M. M.: Influences of changing sea ice and snow thicknesses on simulated Arctic winter heat fluxes, The Cryosphere, 16, 1483–1495, https://doi.org/10.5194/tc-16-1483-2022, 2022.

Lauderdale, J. M., Williams, R. G., Munday, D. R., and Marshall, D. P.: The impact of Southern Ocean residual upwelling on atmospheric CO_2 on centennial and millennial timescales, Clim Dyn, 48, 1611–1631, https://doi.org/10.1007/s00382-016-3163-y, 2017.

Lawrence, D. M., Oleson, K. W., Flanner, M. G., Thornton, P. E., Swenson, S. C., Lawrence, P. J., Zeng, X., Yang, Z.-L., Levis, S., Sakaguchi, K., Bonan, G. B., and Slater, A. G.: Parameterization improvements and functional and structural

https://doi.org/10.5194/egusphere-2026-3834
Preprint. Discussion started: 8 July 2026

advances in Version 4 of the Community Land Model, J. Adv. Model. Earth Syst., 3, M03001, https://doi.org/10.1029/2011MS00045, 2011.

Lhardy, F., Bouttes, N., Roche, D. M., Crosta, X., Waelbroeck, C., and Paillard, D.: Impact of Southern Ocean surface conditions on deep ocean circulation during the LGM: a model analysis, Clim. Past, 17, 1139–1159, https://doi.org/10.5194/cp-17-1139-2021, 2021.

Lindzen, R. S. and Farrell, B.: A Simple Approximate Result for the Maximum Growth Rate of Baroclinic Instabilities, J. Atmos. Sci., 37, 1648–1654, https://doi.org/10.1175/1520-0469(1980)037%3C1648:ASARFT%3E2.0.CO;2, 1980.

Lovenduski, N. S., Gruber, N., Doney, S. C., and Lima, I. D.: Enhanced CO_2 outgassing in the Southern Ocean from a positive phase of the Southern Annular Mode, Global Biogeochemical Cycles, 21, 2006GB002900, https://doi.org/10.1029/2006GB002900, 2007.

Marshall, G. J.: Trends in the Southern Annular Mode from Observations and Reanalyses, J. Climate, 16, 4134–4143, https://doi.org/10.1175/1520-0442(2003)016%3C4134:TITSAM%3E2.0.CO;2, 2003.

Marshall, J. and Speer, K.: Closure of the meridional overturning circulation through Southern Ocean upwelling, Nature Geosci, 5, 171–180, https://doi.org/10.1038/ngeo1391, 2012.

Marzocchi, A. and Jansen, M. F.: Global cooling linked to increased glacial carbon storage via changes in Antarctic sea ice, Nat. Geosci., 12, 1001–1005, https://doi.org/10.1038/s41561-019-0466-8, 2019.

Maykut, G. A.: The surface heat and mass balance, in: The Geophysics of Sea Ice, edited by: Untersteiner, N., NATO ASI Series, Springer, Boston, MA, 395–463, https://doi.org/10.1007/978-1-4899-5352-0_6, 1986.

Menéndez, C. G., Serafini, V., and Le Treut, H.: The effect of sea-ice on the transient atmospheric eddies of the Southern Hemisphere, Climate Dynamics, 15, 659–671, https://doi.org/10.1007/s003820050308, 1999.

Menviel, L. and Spence, P.: Southern Ocean circulation's impact on atmospheric CO_2 concentration, Front. Mar. Sci., 10, https://doi.org/10.3389/fmars.2023.1328534, 2024.

https://doi.org/10.5194/egusphere-2026-3834
Preprint. Discussion started: 8 July 2026

Menviel, L., Timmermann, A., Mouchet, A., and Timm, O.: Climate and marine carbon cycle response to changes in the strength of the Southern Hemispheric westerlies, Paleoceanography, 23, 2008PA001604, https://doi.org/10.1029/2008PA001604, 2008.

Mitchell, J. F. B. and Senior, C. A.: The antarctic winter; simulations with climatological and reduced sea-ice extents, Quart J Royal Meteoro Soc, 115, 225–246, https://doi.org/10.1002/qj.49711548602, 1989.

Monnin, E., Indermühle, A., Dällenbach, A., Flückiger, J., Stauffer, B., Stocker, T. F., Raynaud, D., and Barnola, J.-M.: Atmospheric CO_2 Concentrations over the Last Glacial Termination, Science, 291, 112–114, https://doi.org/10.1126/science.291.5501.112, 2001.

Nadeau, L.-P., Ferrari, R., and Jansen, M. F.: Antarctic Sea Ice Control on the Depth of North Atlantic Deep Water, Journal of Climate, 32, 2537–2551, https://doi.org/10.1175/JCLI-D-18-0519.1, 2019.

Neale, R. B., Chen, C.-C., Gettelman, A., Lauritzen, P. H., Park, S., Williamson, D. L., Conley, A. J., Garcia, R., Kinnison, D., Lamarque, J.-F., Marsh, D. R., Mills, M. J., Smith, A. K., Tilmes, S., Vitt, F., Morrison, H., Cameron-Smith, P., Collins, W. D., Iacono, M. J., Easter, R. C., Ghan, S. J., Liu, X., Rasch, P. J., and Taylor, M. A.: Description of the NCAR Community Atmosphere Model (CAM 5.0), NCAR Tech. Note NCAR/TN-486+STR, National Center for Atmospheric Research, 2012.

Neale, R. B., Richter, J. H., Conley, A. J., Park, S., Lauritzen, P. H., Gettelman, A., Williamson, D. L., Rasch, P. J., Vavrus, S. J., Taylor, M. A., Collins, W. D., Zhang, M., and Lin, S.-J.: Description of the NCAR Community Atmosphere Model (CAM 4.0), NCAR Tech. Note NCAR/TN-485+STR, National Center for Atmospheric Research, 2010.

O'Connor, G. K., Steig, E. J., and Hakim, G. J.: Strengthening Southern Hemisphere Westerlies and Amundsen Sea Low Deepening Over the 20th Century Revealed by Proxy-Data Assimilation, Geophysical Research Letters, 48, e2021GL095999, https://doi.org/10.1029/2021GL095999, 2021.

Oleson, K. W., Lawrence, D. M., Bonan, G. B., Flanner, M. G., Kluzek, E., Lawrence, P. J., Levis, S., Swenson, S. C., Thornton, P. E., Dai, A., Decker, M., Dickinson, R. E., Feddema, J., Heald, C. L., Hoffman, F., Lamarque, J.-F., Mahowald, N., Niu, G.-Y., Qian, T., Randerson, J., Samuelsson, P., Stockli, R., Wang, Y., Yang, Z.-L., Zeng, X., and Zhao, M.: Technical description of version 4.0 of the Community Land Model (CLM), NCAR Tech. Note NCAR/TN-478+STR, 257 pp., National Center for Atmospheric Research, 2010.

https://doi.org/10.5194/egusphere-2026-3834
Preprint. Discussion started: 8 July 2026

Omta, A. W., Follett, C. L., Lauderdale, J. M., and Ferrari, R.: Carbon isotope budget indicates biological disequilibrium dominated ocean carbon storage at the Last Glacial Maximum, Nat Commun, 15, 8006, https://doi.org/10.1038/s41467-024-52360-z, 2024.

Otto-Bliesner, B. L., Brady, E. C., Clauzet, G., Tomas, R., Levis, S., and Kothavala, Z.: Last Glacial Maximum and Holocene Climate in CCSM3, Journal of Climate, 19, 2526–2544, https://doi.org/10.1175/jcli3748.1, 2006.

Perren, B., Kaiser, J., Arz, H., Dellwig, O., Hodgson, D., and Lamy, F.: Fossil diatom and geochemistry data from an 11,000 year lake sediment core from Isla Hornos, Cape Horn Archipelago (1.0), https://doi.org/10.5285/EBB9D50F-94FB-446B-8E90-DE91B3201650, 2025.

Perren, B. B., Hodgson, D. A., Roberts, S. J., Sime, L., Van Nieuwenhuyze, W., Verleyen, E., and Vyverman, W.: Southward migration of the Southern Hemisphere westerly winds corresponds with warming climate over centennial timescales, Commun Earth Environ, 1, https://doi.org/10.1038/s43247-020-00059-6, 2020.

Quade, J. and Kaplan, M. R.: Lake-level stratigraphy and geochronology revisited at Lago (Lake) Cardiel, Argentina, and changes in the Southern Hemispheric Westerlies over the last 25 ka, Quaternary Science Reviews, 177, 173–188, https://doi.org/10.1016/j.quascirev.2017.10.006, 2017.

Rayner, N. A., Parker, D. E., Horton, E. B., Folland, C. K., Alexander, L. V., Rowell, D. P., Kent, E. C., and Kaplan, A.: Global analyses of sea surface temperature, sea ice, and night marine air temperature since the late nineteenth century, J. Geophys. Res., 108, 2002JD002670, https://doi.org/10.1029/2002JD002670, 2003.

Rintoul, S. R.: The global influence of localized dynamics in the Southern Ocean, Nature, 558, 209–218, https://doi.org/10.1038/s41586-018-0182-3, 2018.

Rojas, M.: Sensitivity of Southern Hemisphere circulation to LGM and 4 × CO2 climates, Geophysical Research Letters, 40, 965–970, https://doi.org/10.1002/grl.50195, 2013.

Rojas, M., Moreno, P., Kageyama, M., Crucifix, M., Hewitt, C., Abe-Ouchi, A., Ohgaito, R., Brady, E. C., and Hope, P.: The Southern Westerlies during the last glacial maximum in PMIP2 simulations, Clim Dyn, 32, 525–548, https://doi.org/10.1007/s00382-008-0421-7, 2009.

https://doi.org/10.5194/egusphere-2026-3834
Preprint. Discussion started: 8 July 2026

Santer, B. D., Taylor, K. E., Wigley, T. M. L., Johns, T. C., Jones, P. D., Karoly, D. J., Mitchell, J. F. B., Oort, A. H., Penner, J. E., Ramaswamy, V., Schwarzkopf, M. D., Stouffer, R. J., and Tett, S.: A search for human influences on the thermal structure of the atmosphere, Nature, 382, 39–46, https://doi.org/10.1038/382039a0, 1996.

Santer, B. D., Wigley, T. M. L., Mears, C., Wentz, F. J., Klein, S. A., Seidel, D. J., Taylor, K. E., Thorne, P. W., Wehner, M. F., Gleckler, P. J., Boyle, J. S., Collins, W. D., Dixon, K. W., Doutriaux, C., Free, M., Fu, Q., Hansen, J. E., Jones, G. S., Ruedy, R., Karl, T. R., Lanzante, J. R., Meehl, G. A., Ramaswamy, V., Russell, G., and Schmidt, G. A.: Amplification of Surface Temperature Trends and Variability in the Tropical Atmosphere, Science, 309, 1551–1556, https://doi.org/10.1126/science.1114867, 2005.

Saunders, K. M., Kamenik, C., Hodgson, D. A., Hunziker, S., Siffert, L., Fischer, D., Fujak, M., Gibson, J. A. E., and Grosjean, M.: Late Holocene changes in precipitation in northwest Tasmania and their potential links to shifts in the Southern Hemisphere westerly winds, Global and Planetary Change, 92–93, 82–91, https://doi.org/10.1016/j.gloplacha.2012.04.005, 2012.

Saunders, K. M., Roberts, S. J., Perren, B., Butz, C., Sime, L., Davies, S., Van Nieuwenhuyze, W., Grosjean, M., and Hodgson, D. A.: Holocene dynamics of the Southern Hemisphere westerly winds and possible links to CO_2 outgassing, Nature Geosci, 11, 650–655, https://doi.org/10.1038/s41561-018-0186-5, 2018.

Screen, J. A., Deser, C., Smith, D. M., Zhang, X., Blackport, R., Kushner, P. J., Oudar, T., McCusker, K. E., and Sun, L.: Consistency and discrepancy in the atmospheric response toArctic sea-ice loss across climate models, Nature Geosci, 11, 155–163, https://doi.org/10.1038/s41561-018-0059-y, 2018.

Screen, J. A., Eade, R., Smith, D. M., Thomson, S., and Yu, H.: Net Equatorward Shift of the Jet Streams When the Contribution From Sea-Ice Loss Is Constrained by Observed Eddy Feedback, Geophysical Research Letters, 49, e2022GL100523, https://doi.org/10.1029/2022GL100523, 2022.

Sherriff-Tadano, S., Abe-Ouchi, A., Yoshimori, M., Ohgaito, R., Vadsaria, T., Chan, W.-L., Hotta, H., Kikuchi, M., Kodama, T., Oka, A., and Suzuki, K.: Southern Ocean Surface Temperatures and Cloud Biases in Climate Models Connected to the Representation of Glacial Deep Ocean Circulation, Journal of Climate, 36, 3849–3866, https://doi.org/10.1175/JCLI-D-22-0221.1, 2023.

Sime, L. C., Kohfeld, K. E., Le Quéré, C., Wolff, E. W., De Boer, A. M., Graham, R. M., and Bopp, L.: Southern Hemisphere westerly wind changes during the Last Glacial Maximum: model-data comparison, Quaternary Science Reviews, 64, 104–120, https://doi.org/10.1016/j.quascirev.2012.12.008, 2013.

https://doi.org/10.5194/egusphere-2026-3834
Preprint. Discussion started: 8 July 2026

Sime, L. C., Hodgson, D., Bracegirdle, T. J., Allen, C., Perren, B., Roberts, S., and De Boer, A. M.: Sea ice led to poleward-shifted winds at the Last Glacial Maximum: the influence of state dependency on CMIP5 and PMIP3 models, Clim. Past, 12, 2241–2253, https://doi.org/10.5194/cp-12-2241-2016, 2016.

Simpkins, G. R., Ciasto, L. M., Thompson, David. W. J., and England, M. H.: Seasonal Relationships between Large-Scale Climate Variability and Antarctic Sea Ice Concentration, Journal of Climate, 25, 5451–5469, https://doi.org/10.1175/JCLI-D-11-00367.1, 2012.

Smith, R., Jones, P., Briegleb, B., Bryan, F., Danabasoglu, G., Dennis, J., Dukowicz, J., Eden, C., Fox-Kemper, B., Gent, P., Hecht, M., Jayne, S., Jochum, M., Large, W., Lindsay, K., Maltrud, M., Norton, N., Peacock, S., Vertenstein, M., and Yeager, S.: The Parallel Ocean Program (POP) Reference Manual Ocean Component of the Community Climate System Model (CCSM), Los Alamos National Laboratory Tech. Rep. LA-UR-10-01853, 2010.

Son, S. -W., Gerber, E. P., Perlwitz, J., Polvani, L. M., Gillett, N. P., Seo, K. -H., Eyring, V., Shepherd, T. G., Waugh, D., Akiyoshi, H., Austin, J., Baumgaertner, A., Bekki, S., Braesicke, P., Brühl, C., Butchart, N., Chipperfield, M. P., Cugnet, D., Dameris, M., Dhomse, S., Frith, S., Garny, H., Garcia, R., Hardiman, S. C., Jöckel, P., Lamarque, J. F., Mancini, E., Marchand, M., Michou, M., Nakamura, T., Morgenstern, O., Pitari, G., Plummer, D. A., Pyle, J., Rozanov, E., Scinocca, J. F., Shibata, K., Smale, D., Teyssèdre, H., Tian, W., and Yamashita, Y.: Impact of stratospheric ozone on Southern Hemisphere circulation change: A multimodel assessment, J. Geophys. Res., 115, 2010JD014271, https://doi.org/10.1029/2010JD014271, 2010.

Son, S.-W., Polvani, L. M., Waugh, D. W., Akiyoshi, H., Garcia, R., Kinnison, D., Pawson, S., Rozanov, E., Shepherd, T. G., and Shibata, K.: The Impact of Stratospheric Ozone Recovery on the Southern Hemisphere Westerly Jet, Science, 320, 1486–1489, https://doi.org/10.1126/science.1155939, 2008.

Spoth, M., Hall, B., Lowell, T., Diefendorf, A. F., Corcoran, M. C., and Brickle, P.: Tracking the southern hemisphere westerlies during and since the last glacial maximum with multiproxy lake records from the Falkland Islands (52 °S), Quaternary Science Reviews, 311, 108135, https://doi.org/10.1016/j.quascirev.2023.108135, 2023.

Stein, K., Timmermann, A., Kwon, E. Y., and Friedrich, T.: Timing and magnitude of Southern Ocean sea ice/carbon cycle feedbacks, Proc. Natl. Acad. Sci. U.S.A., 117, 4498–4504, https://doi.org/10.1073/pnas.1908670117, 2020.

Stephens, B. B. and Keeling, R. F.: The influence of Antarctic sea ice on glacial–interglacial CO_2 variations, Nature, 404, 171–174, https://doi.org/10.1038/35004556, 2000.

https://doi.org/10.5194/egusphere-2026-3834
Preprint. Discussion started: 8 July 2026

Swart, N. C. and Fyfe, J. C.: Observed and simulated changes in the Southern Hemisphere surface westerly wind-stress, Geophysical Research Letters, 39, https://doi.org/10.1029/2012gl052810, 2012.

Taylor, K. E., Stouffer, R. J., and Meehl, G. A.: An Overview of CMIP5 and the Experiment Design, Bulletin of the American Meteorological Society, 93, 485–498, https://doi.org/10.1175/BAMS-D-11-00094.1, 2012.

Tetzner, D. R., Allen, C. S., Thomas, E. R., Wolff, E. W., and Franzke, C. L. E.: Timing of the Recent Migration and Intensification of the Southern Hemisphere Westerly Winds, Geophysical Research Letters, 52, e2024GL113672, https://doi.org/10.1029/2024GL113672, 2025.

Thompson, D. W. J. and Solomon, S.: Interpretation of Recent Southern Hemisphere Climate Change, Science, 296, 895–899, https://doi.org/10.1126/science.1069270, 2002.

Thompson, D. W. J., Solomon, S., Kushner, P. J., England, M. H., Grise, K. M., and Karoly, D. J.: Signatures of the Antarctic ozone hole in Southern Hemisphere surface climate change, Nature Geosci, 4, 741–749, https://doi.org/10.1038/ngeo1296, 2011.

Tierney, J. E., Zhu, J., King, J., Malevich, S. B., Hakim, G. J., and Poulsen, C. J.: Glacial cooling and climate sensitivity revisited, Nature, 584, 569–573, https://doi.org/10.1038/s41586-020-2617-x, 2020a.

Tierney, J. E., Poulsen, C. J., Montañez, I. P., Bhattacharya, T., Feng, R., Ford, H. L., Hönisch, B., Inglis, G. N., Petersen, S. V., Sagoo, N., Tabor, C. R., Thirumalai, K., Zhu, J., Burls, N. J., Foster, G. L., Goddéris, Y., Huber, B. T., Ivany, L. C., Kirtland Turner, S., Lunt, D. J., McElwain, J. C., Mills, B. J. W., Otto-Bliesner, B. L., Ridgwell, A., and Zhang, Y. G.: Past climates inform our future, Science, 370, eaay3701, https://doi.org/10.1126/science.aay3701, 2020b.

Toggweiler, J. R. and Russell, J.: Ocean circulation in a warming climate, Nature, 451, 286–288, https://doi.org/10.1038/nature06590, 2008.

Toggweiler, J. R. and Samuels, B.: Effect of drake passage on the global thermohaline circulation, Deep Sea Research Part I: Oceanographic Research Papers, 42, 477–500, https://doi.org/10.1016/0967-0637(95)00012-U, 1995.

Toggweiler, J. R., Russell, J. L., and Carson, S. R.: Midlatitude westerlies, atmospheric CO_2 , and climate change during the ice ages, Paleoceanography, 21, 2005PA001154, https://doi.org/10.1029/2005PA001154, 2006.

https://doi.org/10.5194/egusphere-2026-3834
Preprint. Discussion started: 8 July 2026

Vallis, G. K.: Atmospheric and Oceanic Fluid Dynamics: Fundamentals and Large-Scale Circulation, 2nd edn., Cambridge University Press, 946 pp., https://doi.org/10.1017/9781107588417, 2017.

Visbeck, M.: A Station-Based Southern Annular Mode Index from 1884 to 2005, Journal of Climate, 22, 940–950, https://doi.org/10.1175/2008JCLI2260.1, 2009.

Wyrwoll, K.-H., Dong, B., and Valdes, P.: On the position of southern hemisphere westerlies at the Last Glacial Maximum: an outline of AGCM simulation results and evaluation of their implications, Quaternary Science Reviews, 19, 881–898, https://doi.org/10.1016/S0277-3791(99)00047-5, 2000.

Yin, J. H.: A consistent poleward shift of the storm tracks in simulations of 21st century climate, Geophysical Research Letters, 32, 2005GL023684, https://doi.org/10.1029/2005GL023684, 2005.

Young, I. R. and Ribal, A.: Multiplatform evaluation of global trends in wind speed and wave height, Science, 364, 548–552, https://doi.org/10.1126/science.aav9527, 2019.

Zheng, F., Li, J., Clark, R. T., and Nnamchi, H. C.: Simulation and Projection of the Southern Hemisphere Annular Mode in CMIP5 Models, Journal of Climate, 26, 9860–9879, https://doi.org/10.1175/JCLI-D-13-00204.1, 2013.

Zhu, J. and Poulsen, C. J.: Last Glacial Maximum (LGM) climate forcing and ocean dynamical feedback and their implications for estimating climate sensitivity, Clim. Past, 17, 253–267, https://doi.org/10.5194/cp-17-253-2021, 2021.